# CHAPTER 4

# RESULTS & DISCUSSIONS

CHAPTER 4

# Section A: Phenol biodegradation

### 4.1. Selection of potential microbial species

The phenol removal efficiency (RE) of each isolated microbial species (GS1, GS2, GS3, GS4, GS5, and GS6) were evaluated and represented in Figure 4.1. It was found that the microbial species named GS1 could able to remove maximum phenol of 89.44 %. However, 79.3, 60.05, 70.12, 40.22, and 54.28 % REs were obtained by GS2, GS3, GS4, GS5, and GS6, respectively. The GS1 and GS2 were selected for the identification and used for the biodegradation of phenol and its derivatives in this work.

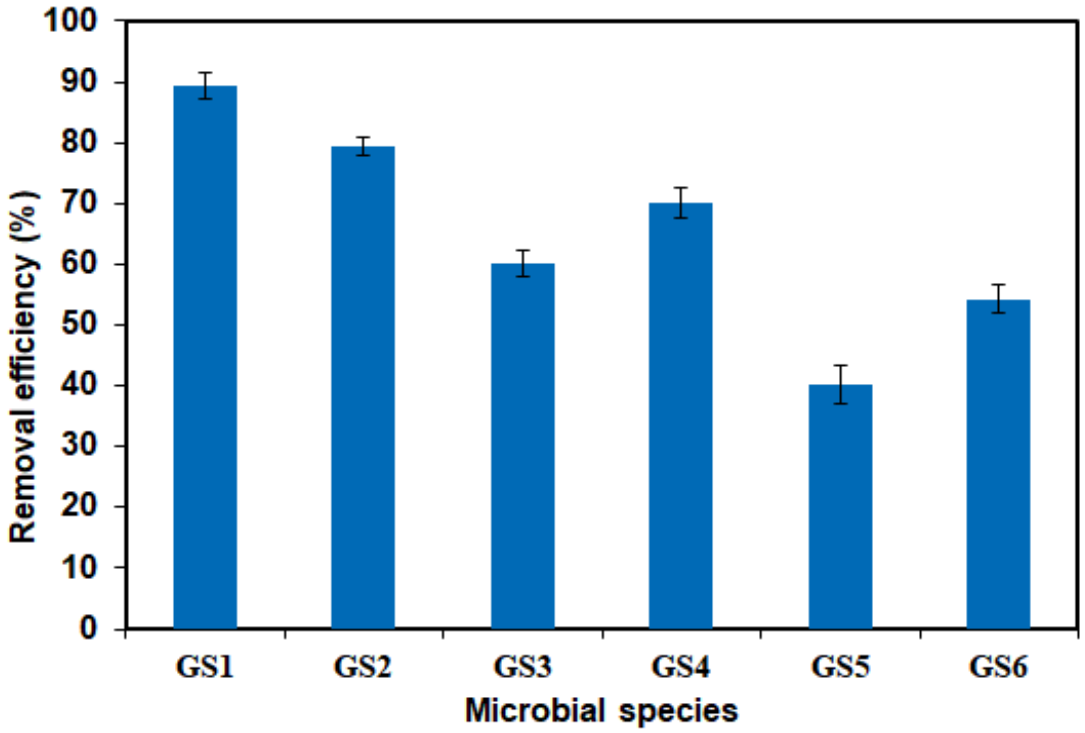


**Figure 4.1.** Schematic representation of removal efficiency of phenol by isolated microbial species (phenol concentration = 100 mg/L, pH = 7.0, temperature = 35 °C, time = 10 days)

### 4.2. Identification of microbial species

The characterization of the potential species was carried out at Triyat Scientific, Nagpur, India. The DNA amplification was carried out by polymerase chain reaction (PCR) method using primers 8F (5'AGAGTTTGATCCTGGCTCAG3') and 1541R (5'AAGGAGGTGATCCAGCCGCA3'). The PCR was performed using the following thermal cycling conditions: initial denaturation at 95 ºC for 2 min, denaturation at 95 ºC for 30 sec, annealing 55 ºC for 30 sec, and extension at 72 ºC for 2 min, respectively. Single-pass sequencing was performed in electrophoresis using an ABI 3730xl sequencer. The 16s rRNA sequence with accession numbers MK850444.1 and MN966874.1 were blast using the NCBI similarity search tool. These species were identified as *Bacillus flexus* GS1 IIT (BHU) and *Bacillus cereus* GS2 IIT (BHU). The program MUSCLE 3.7 was used for multiple alignments of sequences and the constructed phylogenetic trees were represented in Figure 4.2.

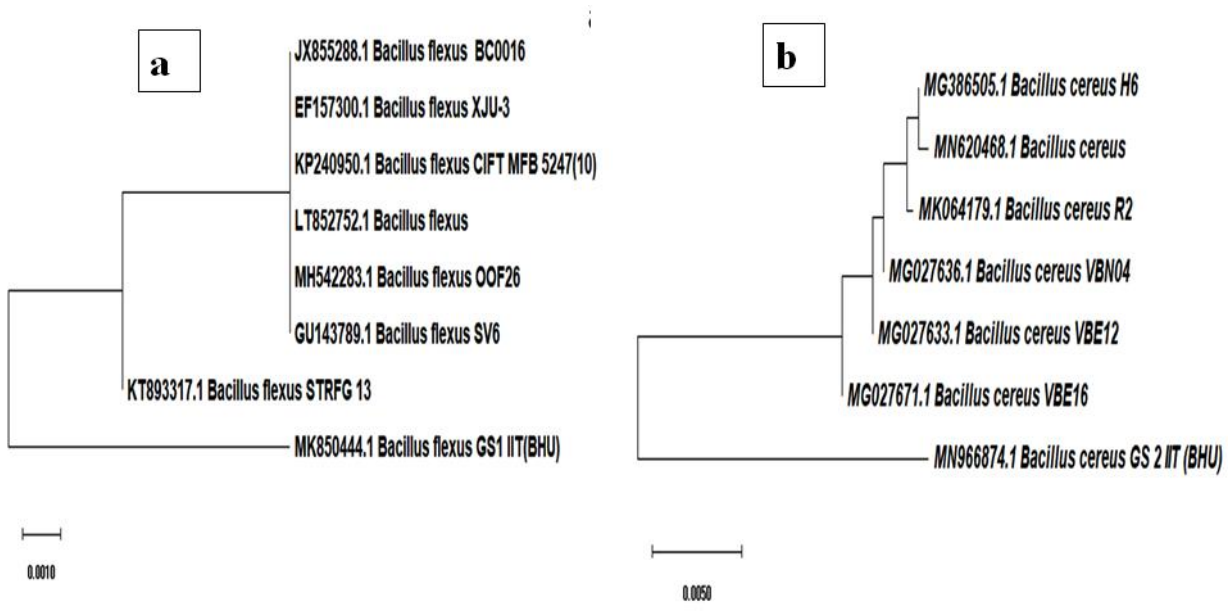


**Figure 4.2.** Phylogenetic tree of isolated bacterial species *Bacillus flexus* GS1 IIT (BHU) (MK850444.1) for biodegradation of phenol.

### 4.3. Process variables optimization in free cell system

#### 4.3.1. Effect of pH

The pH of the wastewater plays an important role during the biodegradation process as it controls the metabolic activity of the bacterial species. The significant removal efficiency (RE) of phenol was observed in the pH range of 6.0-8.0. It was observed that the highest phenol RE was obtained at a pH of 7.0 and found to be 84.51 % (Figure 4.3). Then it decreased to 52.68% with an increase in pH up to 9.0. Biodegradation of phenol was obtained to be 41.04 % when the pH of the media decreased to 5.0. The phenol RE was continuously decreased at highly acidic or alkaline conditions. At acidic or alkaline pH, the hydroxyl and proton radicals may adversely affect the enzymatic activity of *Bacillus* species. The optical density ($OD_{600}$) was measured to evaluate the bacterial growth at each condition. The bacterial growth was found to be declined with the change of pH from 7.0. The rate-limiting step is the diffusion of the proton (H+) / hydroxyl (OH-) ions into the cell membrane from the bulk liquid. Moderate changes in surrounding pH can deteriorate the molecular bonding of the bacterial cell.

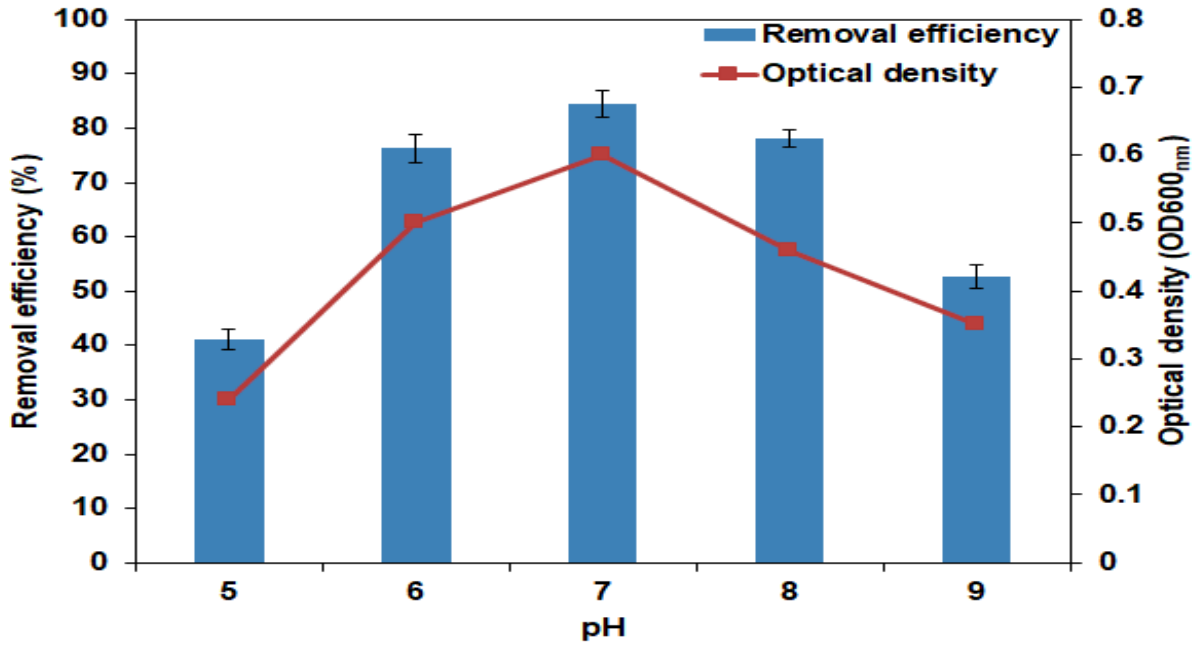

**Figure 4.3.** Effect of pH on the removal of efficiency phenol in free cell (phenol concentration = 150 mg/L, temperature = 30 ℃).

### 4.3.2. Effect of temperature

Another critical process parameter, i.e., temperature, was optimized by varying between 25-40 ºC and keeping the other parameters constant. The phenol RE was increased with the increase of temperature up to 30 ºC. Maximum phenol REs of 83.59 % was obtained at a temperature of 30 ºC (Figure 4.4). The phenol RE was sharply reduced with further increasing the temperature above 30 ºC. The phenol RE of 80.63 and 48 % were observed at temperatures of 35 and 40 ℃, respectively. In addition, the bacterial growth was inhibited at a high temperature which was responsible for the decrease of optical density. It seems that the increase of temperature beyond 30 ºC may decrease the enzymatic activity during the phenol biodegradation, hence resulting in lower phenol removal efficiency. The intercellular proteins and nucleic acids of bacterial species denature at a high temperature (Sahoo et al., 2011). In addition, the cell membrane and inner cell wall of the bacteria may damage when exposed to a high temperature resulting in the death of the bacterial cell. Therefore, operating the biochemical reactions at an optimal temperature is always favourable for maximum pollutant removal efficiency.

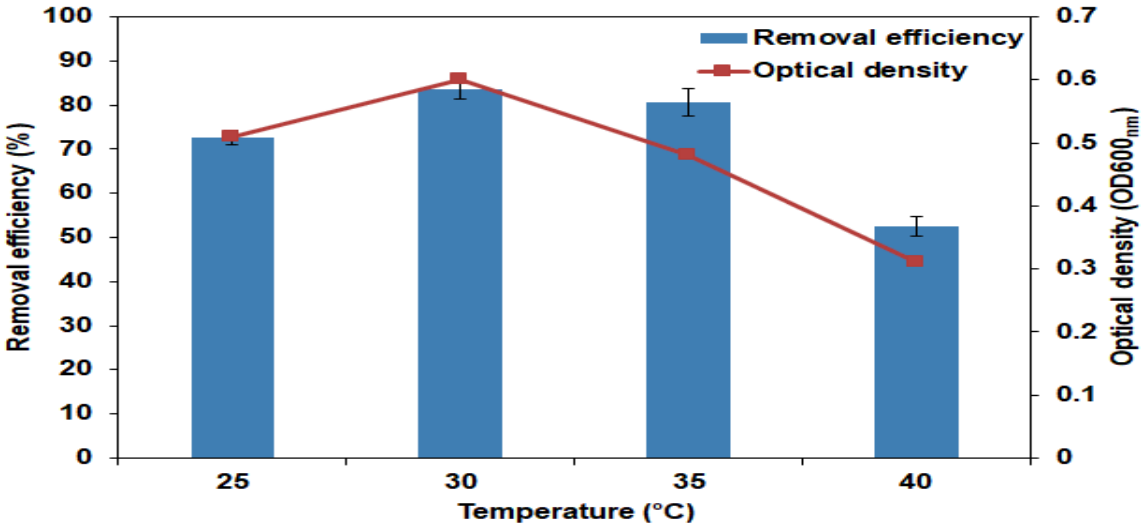

**Figure 4.4.** Effect of temperature on the removal efficiency of phenol in free cell (phenol concentration = 150 mg/L, pH = 7.0).

### 4.3.3. Effect of initial phenol concentration

The impact of the initial phenol concentration (50-500 mg/L) on the RE of phenol was studied at optimized conditions of pH (7.0) and temperature (30 ºC). The maximum RE of 93.02 % was obtained at an initial phenol concentration of 100 mg/L (Figure 4.5). Further, increasing the phenol concentration above 100 mg/L, the RE was continuously decreased, probably due to the substrate inhibition effect. Moreover, the lowest phenol removal of 32.59 % was obtained at the initial concentration of 500 mg/L. Mohanty and Jena (2017) have analysed the effect of initial phenol concentration on the RE in the free cell system. They have reported that low RE was achieved due to the exposure of the microorganisms at a high concentration of phenol which could lead to the death of the microbial cells.

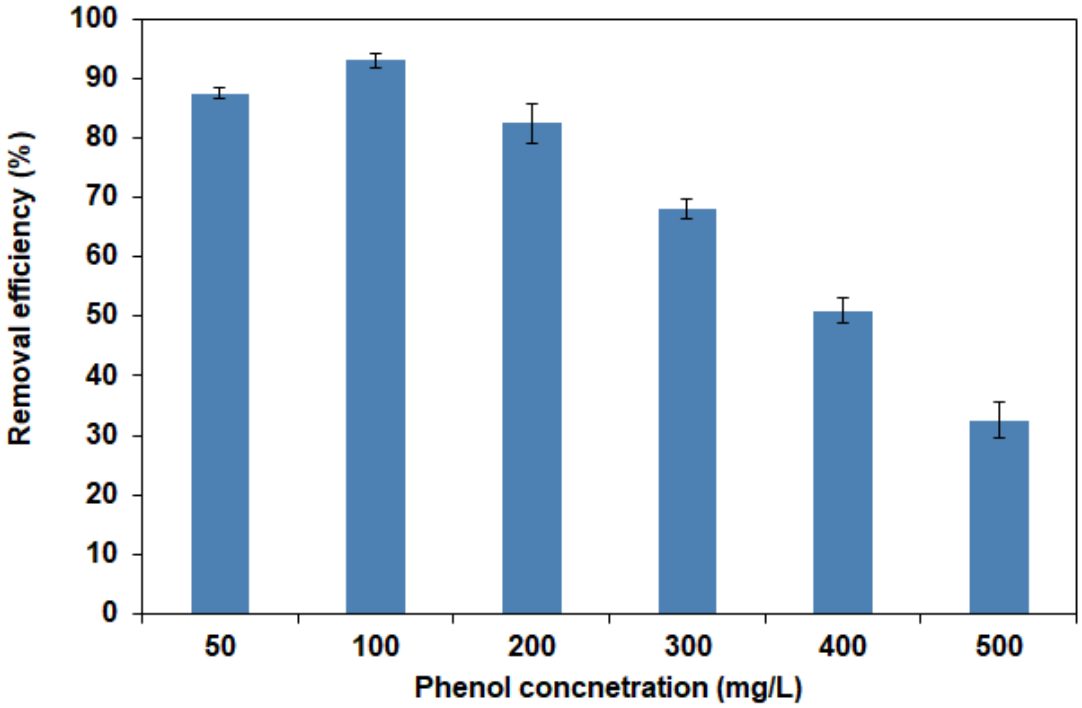


**Figure 4.5.** Effect of the initial phenol concentration on the removal efficiency of phenol in free cell (pH = 7.0, temperature = 30 ℃).

### 4.4. Substrate inhibition models

To evaluate the efficacy of phenol degrading bacteria, two kinetic models, i.e., Monod and Andrew - Haldane, were used. The specific growth rate ($\mu$) of the microorganisms was calculated at different substrate concentrations of range 50 -700 mg/L and plotted against phenol concentration, as shown in Figure 4.6. The specific growth rate of *Bacillus* species increased up to 200 mg/L, and after that, it decreased continuously due to the toxic effect of phenol. At the substrate non-inhibition condition, Monod kinetics well described the efficacy of the microorganisms. The kinetic parameters i.e., $\mu_{max}$ and $K_s$ were calculated and obtained to be 0.214 $h^{-1}$ and 80 mg/L, respectively. The Andrew-Haldane kinetic parameters, i.e., $\mu_{max}$, $K_s$, and $K_i$, were calculated by non-linear regression analysis and found to be 0.328 $h^{-1}$, 69 mg/L, and 194 mg/L, respectively. The calculated values of kinetic parameters were shown in Table 4.1. For the biochemical reaction, high $\mu_{max}$ and low $K_s$ values were always preferred. Hence, the value of $\frac{\mu max}{Ks}$ was taken to be an important parameter in evaluating the potential of substrate degradation capacity. In this study, the values of $\frac{\mu max}{Ks}$ were found to be 0.0027 L $mg^{-1}$ $h^{-1}$ for the Monod model and 0.0047 L $mg^{-1}$ $h^{-1}$ for the Andrew-Haldane model.

**Table 4.1.** Monod and Andrew-Haldane kinetic parameters for biodegradation of phenol.

| Phenol concentration (mg/L | $\mu_{max}$ ($h^{-1}$) | $K_s$ (mg/L) | $K_i$ (mg/L) | $\mu_{max}$/ $K_s$ (L $mg^{-1}h^{-1}$) | $R^2$ |
|---|---|---|---|---|---|
| 50-700 (Monod) | 0.214 | 80 | - | 0.0027 | 0.45 |
| 50-700 (Andrew-Haldane) | 0.328 | 69 | 194 | 0.0047 | 0.98 |

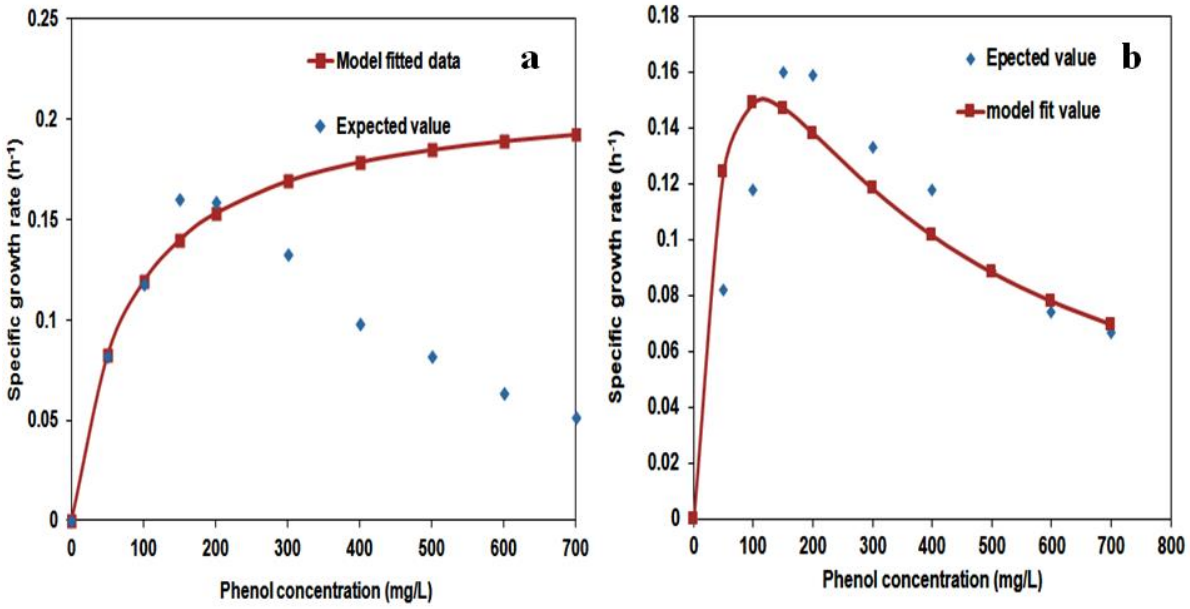


**Figure 4.6.** Graph plotted between specific growth rates against phenol concentrations using (a) Monod model, (b) Andrew-Haldane model.

### 4.5. Phenol biodegradation in a packed bed bioreactor

#### 4.5.1. Morphological characteristics of the biocarrier

The morphology of low-density polyethylene (LDPE) was analysed by scanning electron microscope (SEM) before and after the immobilization of *Bacillus* sp. Before immobilization, several micropores were observed on the surface of LDPE, which was responsible for biofilm growth (Figure 4.7a). However, after immobilization, a layer of biofilm was developed on the surface of LDPE (Figure 4.7b). The biofilm growth mainly depends on the substrate availability, dissolved oxygen, pH of the media, and temperature.

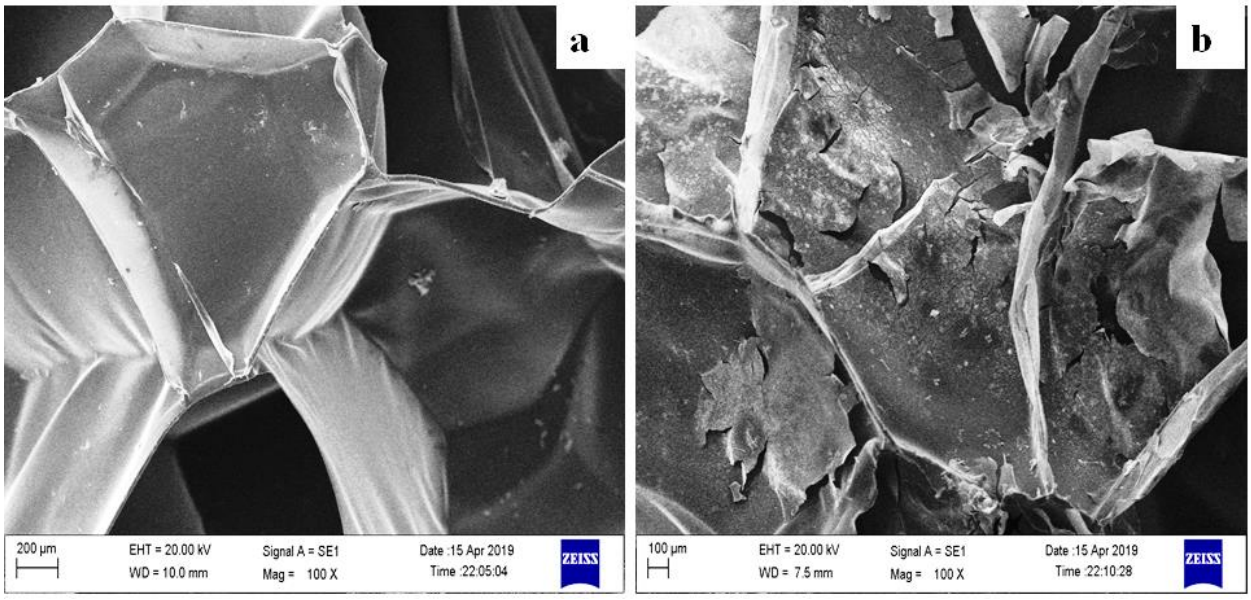


**Figure 4.7.** SEM images of low-density polyethylene (a) before immobilization (blank), (b) after immobilization.

### 4.5.2. Performance evaluation of a continuous packed bed bioreactor

The packed bed bioreactor (PBBR) was operated in a continuous mode by varying the feed flow rate (15 - 60 mL/h) at an initial phenol concentration of 100 mg/L. The pH and temperature were maintained at 7.0 ± 0.2 and 30 ± 3 ºC, respectively. The phenol removal performance of the bioreactor was analysed by evaluating the removal efficiency (RE), elimination capacity (EC), and inlet loading rate (ILR) (Table 4.2) during the operation. In the starting phase, the PBBR was fed with the wastewater at a flow rate of 15 mL/h and an inlet loading rate (ILR) of 36 mg/L/d. The phenol removal efficiency (RE) was gradually increased and attained a maximum value of 99.13 % after 120 h of operation (Figure 4.8). In addition, the maximum elimination capacity (EC) was obtained to be 35.69 mg/L/d. Further, the feed flow rate was switched to 30 mL/h with an ILR of 72 mg/L/d. It was observed that the RE was suddenly decreased to 82.38 % due to the increase in loading rate. However, the RE was increased after that and stabilized at 96.38 % after 250 h. The increment of EC was observed due to the presence of more phenol in the wastewater and found to be 69.34 mg/L/d. In the next stage, the feed flow rate was increased to 45 mL/h. The PBBR was attained a

maximum RE of 90.4 % with an EC of 97.63 mg/L/d on 390$^{th}$ h of operation. The phenol RE was significantly decreased to 65.35 % when the inlet feed rate was increased to 60 mL/h. Then, the bioreactor was stabilized after 504$^{th}$ h of operation. Finally, the maximum RE and EC of 83.7 % and 120.53 mg/L/d were achieved.

Erhan et al. (2004) reported that the phenol RE was drastically reduced from 100 to 82.5 % with the flow rate increase from 0.5 to 10 mL/min in a PBBR. Yadav et al. (2014) had studied the effect of inlet feed flow rate on chlorpyrifos removal in a PBBR. It was revealed that the maximum RE (lower EC) was obtained at a lower feed flow rate and the minimum RE (higher EC) resulted at a higher flow rate of the wastewater. At a higher feed flow rate, entrainment of phenol may be possible from the PBBR without contacting the bacterial cell. The less retention period of the influent in the PBBR was may be responsible for the decline of RE (Banerjee and Ghoshal, 2016; Basak et al., 2019).

**Table 4.2.** Effect of the flow rate and inlet loading rate on removal efficiency and elimination capacity of packed bed bioreactor (PBBR).

| Flow rate (mL/h) | Time (h) | Inlet loading rate (mg/L/ d) | Removal efficiency (%) | Elimination capacity (mg/L/d) |
|---|---|---|---|---|
| 15 | 0-120 | 36 | 99.13 | 35.69 |
| 30 | 125-250 | 72 | 96.38 | 69.34 |
| 45 | 255-390 | 108 | 90.40 | 97.63 |
| 60 | 395-504 | 144 | 83.7 | 120.53 |

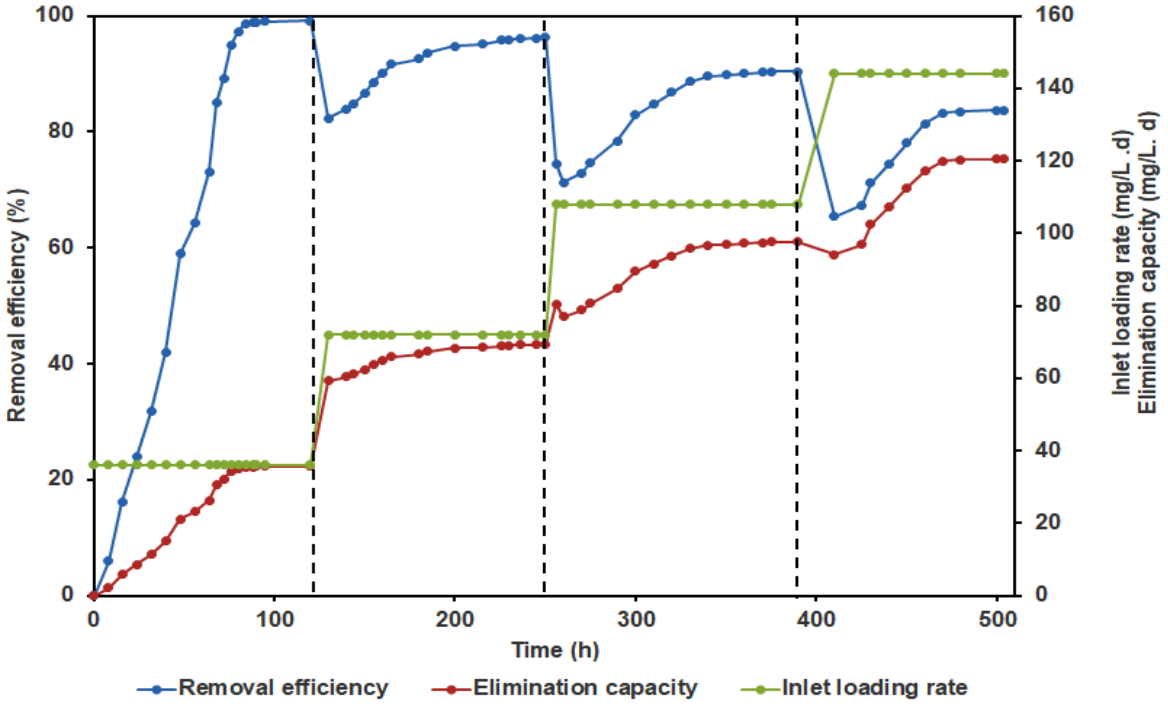


**Figure 4.8.** Effect of various flow rates on removal efficiencies of phenol in a continuously operated packed bed bioreactor; $C_0$ = 100 mg/L, pH= 7.0 ± 0.2, temperature = 30 ± 3 ° C.

### 4.5.3. External mass transfer analysis

The external film diffusion effect on phenol biodegradation rate was studied by determining $N_{Re}$ and $G$ at various feed flow rates (15-60 mL/h) using experimentally calculated data of $d_p$=1 cm, $\rho$=0.996 g/cm$^3$, $\varepsilon$=0.35, $A$=23.76 cm$^2$, $\mu$=0.00843 g/cm s, $D_f$ =9.1 × 10$^{-6}$ cm$^2$/s. The values of $1/k_p$, $G$, $N_{Re}$, $1/G^n$ were evaluated at different values of $n$ ($0<n\leq 1$) and included in Table 4.3. Then, straight-line graphs were plotted against $1/k_p$ vs. $1/G^n$ as per the Eq. (18) and the obtained slopes and intercepts were given in Table 4.4. The n values (<0.33) were ignored due to the negative intercept. The obtained slopes and intercepts were increasing with the increase of $n$. The graphical representations between $1/k_p$ and $1/G^n$ for various values of $n$ (0.33, 0.36, 0.5, 0.7, 0.8, 1.0) were given in Figure 4.9. The high regression coefficients ($R^2$>0.94) showed that the better predictability of the experimental data for all n values. However, it did not imply that every value of $n$ could accurately estimate the experimental mass transfer area ($a_m$). Therefore, various values of $K$ were taken

from the previous studies for further analysis ( Tepe and Dursun, 2008; Banerjee and Ghoshal, 2016). The values of the dimensionless parameter i.e., *N*, were calculated using Eq. (17). The slopes and intercepts obtained from the graphs plotted between $1/k_p$ and $1/G^n$ were used to calculate the available surface area ($a_m$) and $k_s$. From Table 4.5, approximately closed value of $a_m$ was resulted at corresponding values of *K* and *n* of 3.114 and 0.36, respectively, to experimental value (4.14 $cm^2/g$).

The mass transfer coefficients ($k_m$) were evaluated using Eq. (13) at each flow rate and provided in Table 4.6. The $k_m$ values were calculated and obtained to be 1.931, 2.762, 2.964, and 3.071 $mL/cm^2$ h at corresponding flow rates of 15, 30, 45, and 60 mL/h, respectively. It was observed that the external mass transfer coefficient increased with the increase of the flow rate due to high mixing and turbulence (Dizge and Tansel, 2010). The slope (*n*) and intercept (ln*N*) were obtained from the graph between ln$k_m$ and ln*G* give the values of *n* and *N* (Eq. 16). In this study, the slope and the intercept were found to be 0.34 and -6.4467, respectively (Figure 4.10). The value of *N* (0.00158) was determined from the intercept, which was very close to the value obtained at *K*=3.114 (Table 4.5). According to these results, it can be concluded that the mass transfer correlation $J_D = 3.114\mathrm{N_{Re}}^{-0.64}$ anticipates the film diffusion effect accurately for the biodegradation of phenol in LDPE immobilized PBBR. The comparison between the estimated data of $k_p$ with the experimental values at different *n* values is shown in Table 4.7, which represents similar values of $k_p$ at *n*=0.36. From the above results, it can be concluded that the suggested model anticipates the limiting factor of removal of phenol in a PBBR immobilized with *Bacillus* species.

**Table 4.3.** Experimentally calculated values of $k_p$ (obtained from Eq (10)) and measured values of $G$, $1/G^n$, $1/k_p$ at different flow rates.

| $Q$ (mL/h) | $k_p$ (L/g h) | $1/k_p$ (g h/L) | $G$ (g/cm$^2$h) | $1/G^{0.1}$ | $1/G^{0.33}$ | $1/G^{0.35}$ | $1/G^{0.36}$ | $1/G^{0.39}$ | $1/G^{0.4}$ | $1/G^{0.5}$ | $1/G^{0.6}$ | $1/G^{0.7}$ | $1/G^{0.8}$ | $1/G^{0.9}$ | $1/G^{1.0}$ |
|---|---|---|---|---|---|---|---|---|---|---|---|---|---|---|---|
| 15 | 0.0075 | 133.333 | 2.022 | 0.932 | 0.792 | 0.781 | 0.776 | 0.759 | 0.754 | 0.703 | 0.655 | 0.610 | 0.569 | 0.530 | 0.494 |
| 30 | 0.0103 | 97.087 | 4.044 | 0.869 | 0.630 | 0.613 | 0.604 | 0.579 | 0.571 | 0.497 | 0.432 | 0.376 | 0.326 | 0.284 | 0.247 |
| 45 | 0.0111 | 90.090 | 6.066 | 0.835 | 0.551 | 0.532 | 0.522 | 0.495 | 0.486 | 0.405 | 0.339 | 0.283 | 0.236 | 0.197 | 0.164 |
| 60 | 0.0115 | 86.956 | 8.088 | 0.811 | 0.501 | 0.481 | 0.471 | 0.442 | 0.433 | 0.351 | 0.285 | 0.231 | 0.187 | 0.152 | 0.123 |

**Table 4.4.** Slope and intercept obtained from the graph plotted between $1/k_p$ vs. $1/G^n$ at corresponding values of $n$.

| $n$ | 0.1 | 0.3 | 0.35 | 0.36 | 0.39 | 0.4 | 0.5 | 0.6 | 0.7 | 0.8 | 0.9 | 1.0 |
|---|---|---|---|---|---|---|---|---|---|---|---|---|
| Slope | - | - | 158.52 | 156.22 | 150.16 | 148.38 | 135.63 | 128.85 | 125.65 | 124.83 | 125.73 | 127.97 |
| Intercept | Negative | Negative | 6.4418 | 9.1346 | 16.381 | 18.554 | 35.475 | 46.714 | 54.703 | 60.66 | 65.259 | 68.907 |

**Table 4.5.** Evaluated values of $N$, external mass transfer area ($a_m$), intrinsic first-order reaction rate constant ($k_s$) for different values of $n$ and $K$.

| $n$ | $K$=1.34 | | | $K$=1.625 | | | $K$=2.718 | | | $K$=3.114 | | |
|---|---|---|---|---|---|---|---|---|---|---|---|---|
| | $N\times10^4$ | $a_m$ (cm$^2$/g) | $k_s$ (L/cm$^2$ h) | $N\times 10^4$ | $a_m$ (cm$^2$/g) | $k_s$ (L/cm$^2$ h) | $N\times10^4$ | $a_m$ (cm$^2$/g) | $k_s$ (L/cm$^2$ h) | $N\times10^4$ | $a_m$ (cm$^2$/g) | $k_s$ (L/cm$^2$ h) |
| 0.35 | 6.33 | 9.99 | 0.02 | 7.67 | 8.22 | 0.02 | 12.83 | 4.92 | 0.03 | 14.70 | 4.29 | 0.04 |
| 0.36 | 6.64 | 9.66 | 0.01 | 8.05 | 7.96 | 0.01 | 13.46 | 4.76 | 0.02 | 15.42 | 4.15 | 0.03 |
| 0.39 | 7.66 | 8.70 | 0.01 | 9.29 | 7.17 | 0.01 | 15.53 | 4.29 | 0.01 | 17.80 | 3.74 | 0.02 |
| 0.40 | 8.03 | 8.39 | 0.01 | 9.74 | 6.92 | 0.01 | 16.29 | 4.14 | 0.01 | 18.67 | 3.61 | 0.02 |
| 0.50 | 12.96 | 5.69 | 0.01 | 15.71 | 4.69 | 0.01 | 26.28 | 2.81 | 0.01 | 30.11 | 2.45 | 0.01 |
| 0.60 | 20.89 | 3.71 | 0.01 | 25.34 | 3.06 | 0.01 | 42.38 | 1.83 | 0.01 | 48.55 | 1.60 | 0.01 |
| 0.70 | 33.70 | 2.36 | 0.01 | 40.86 | 1.95 | 0.01 | 68.35 | 1.16 | 0.02 | 78.31 | 1.02 | 0.02 |
| 0.80 | 54.35 | 1.47 | 0.01 | 65.90 | 1.22 | 0.01 | 110.23 | 0.73 | 0.02 | 126.29 | 0.63 | 0.03 |

| | | | | | | | | | | | | |
|---|---|---|---|---|---|---|---|---|---|---|---|---|
| 0.90 | 87.65 | 0.91 | 0.02 | 106.29 | 0.75 | 0.02 | 177.78 | 0.45 | 0.03 | 203.68 | 0.39 | 0.04 |
| 1.00 | 141.35 | 0.55 | 0.03 | 171.42 | 0.46 | 0.03 | 286.72 | 0.27 | 0.05 | 328.49 | 0.24 | 0.06 |

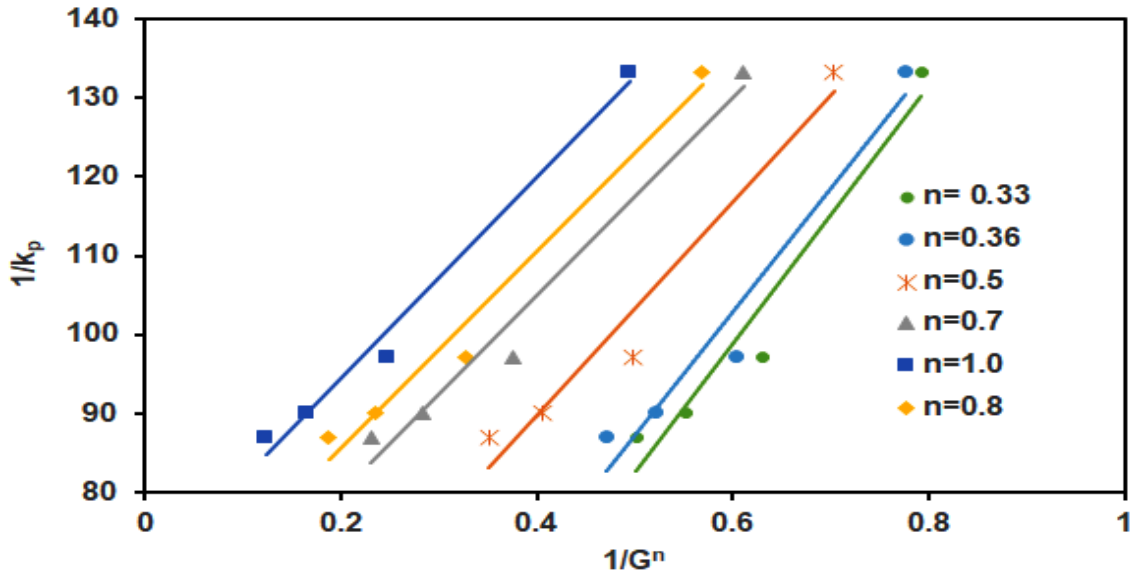


**Figure 4.9.** The straight-line plot between $\frac{1}{k_p}$ against $\frac{1}{G^n}$ for various values of *n* ($R^2$ > 0.95 for all values of n = 0.33, 0.36, 0.5, 0.7, 0.8, 1.0).

**Table 4.6.** Calculated values of mass transfer coefficient ($k_m$) at different mass fluxes ($G$) for $n$= 0.36 and $K$=3.114.

| $Q$ (mL/h) | $G$ (gm/cm$^2$. h) | $k_m \times 10^3$ (L/cm$^2$. h) |
|---|---|---|
| 15 | 2.022 | 1.931 |
| 30 | 4.044 | 2.762 |
| 45 | 6.066 | 2.964 |
| 60 | 8.088 | 3.071 |

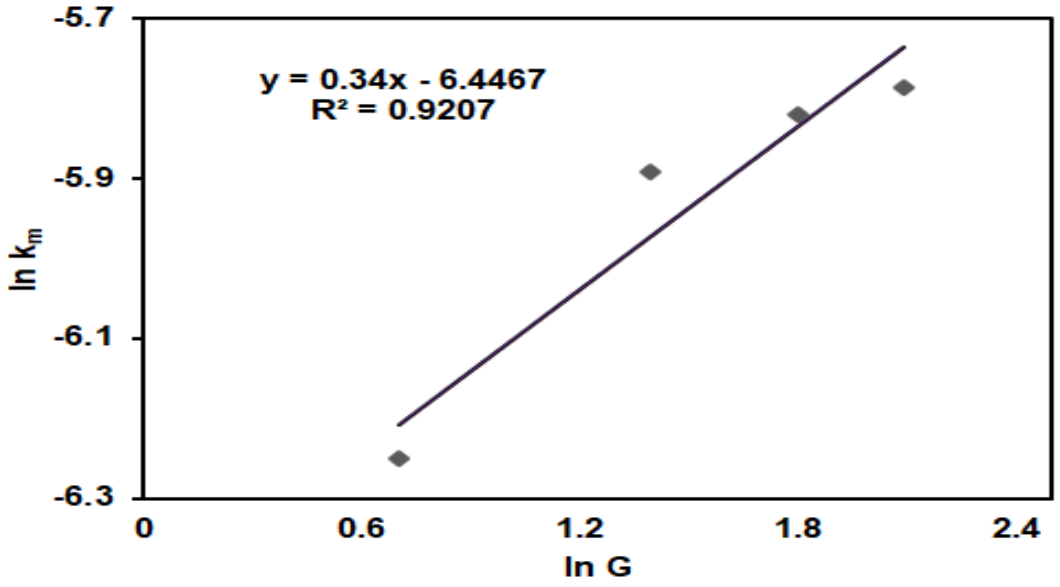


**Figure 4.10.** The plot of ln $K_m$ vs. ln $G$ for evaluation of $N$ and $n$.

**Table 4.7.** Comparison data of $k_p$ values obtained from Eq (10) to those ones calculated from Eq (18) for different values of $n$.

| $Q$ (mL/h) | $k_p$ from Eq (4) (L/g h) | $k_p$ (L/g h) | | | | |
|---|---|---|---|---|---|---|
| | | $n$=0.36 | $n$=0.7 | $n$=0.8 | $n$=0.9 | $n$=1.0 |
| 15 | 0.0075 | 0.0078 | 0.0087 | 0.0092 | 0.00964 | 0.01 |
| 30 | 0.0103 | 0.0099 | 0.0119 | 0.0129 | 0.0139 | 0.0148 |
| 45 | 0.0111 | 0.0111 | 0.0139 | 0.0152 | 0.0164 | 0.0177 |
| 60 | 0.0115 | 0.0124 | 0.01536 | 0.01682 | 0.0182 | 0.0195 |

### 4.6. Phenol biodegradation in a moving bed biofilm reactor

#### 4.6.1. Morphological characteristics of the biofilm carrier

The morphology of the modified carriers (PP-PUF) before ($0^{th}$ day) and after immobilization ($15^{th}$ day) were examined by SEM (Figure 4.11). The number of micropores ($0^{th}$ day) were found on the surface of carriers to provide large surface area for the biofilm formation. However, the dense biofilm was observed on the surface of the carrier after 15 days. The growth of biofilm generally depends upon the concentration of carbon source, pH of the growth media, and temperature. The average biomass concentration attached to PP-PUF carriers in this study was measured to be as 2.38g VSS/L. This high biomass attached to the carriers would enable the efficient removal of phenol, COD, and ammonia.

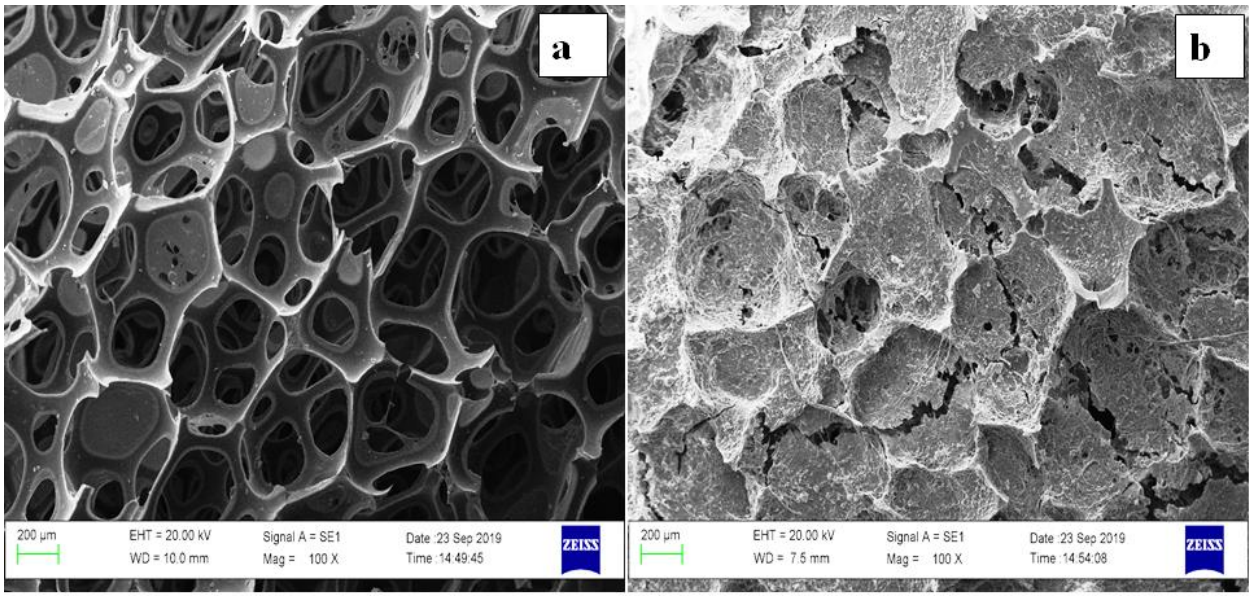


**Figure 4.11.** SEM images of PP-PUF (a) before immobilization (b) after immobilization.

### 4.6.2. Optimization of pH, HRT, and air flow rate by using RSM technique

#### 4.6.2.1. Process optimization

The independent process variables such as pH (5.0 – 8.0), retention time (RT: 2.0 -12.0 h), and airflow rate (AFR: 0.8 -3.5 L/min) were selected for the optimization study. The removal of phenol, chemical oxygen demand (COD), and ammonia were taken as response variables. The relationship between the independent process variables and the responses was examined by performing total 20 experiments, and the summary of outcomes was given in Table 4.8. The validations of different regression models were performed, and the quadratic model was found to fit appropriately with the obtained data. Finally, the values of $R^2$, adjusted $R^2$, and predicted $R^2$ evaluated using the quadratic models were summarized in Table 4.9. The values of adjusted $R^2$ were obtained as 0.980, 0.969, and 0.909 for phenol, COD, and ammonia removal, respectively. Similarly, the values of predicted $R^2$ were found to be 0.915, 0.877, and 0.721 for phenol, COD, and ammonia removal, respectively. The obtained values of $R^2$ being greater than 0.9 and the difference between adjusted $R^2$ and predicted $R^2$ being less than 0.2 signifies that the quadratic model was suitable for the obtained data.

#### 4.6.2.2. Effect of process variables on phenol and ammonia removal

The process variables such as pH, retention time, and airflow rate play a significant role in phenol, COD, and ammonia removal. The removal of phenol, COD, and ammonia increased with increasing the pH from 5.0 to 6.5. Upon further increase in the pH level, the removal efficiency started decreasing (Figure 4.12). The removal efficiencies of phenol were obtained to be 61.7, 92.2, and 62.2% at a pH of 5.0, 6.5, and 8.0, respectively (at RT = 7.0 h and AFR = 2.15 L/min) (Table 4.8). The removal efficiencies of COD were found as 52, 72.1, and 65.2 % at a pH of 5.0, 6.5, and 8.0, respectively. Similarly, the high removal efficiency of ammonia was obtained as 91.2 % at pH 6.5. Hence, the optimum pH for the collective

removal of phenol, COD, and ammonia was obtained around 6.5. This is because a highly acidic or alkaline medium inhibits bacterial growth due to reduced enzymatic activity, which, in turn, results in low removal efficiency of the pollutants.

It was found that the removal of phenol, COD, and ammonia increased with increasing the process time, and reached the level of 93.1, 72.8, and 91.2%, respectively, in 7.0 h (at pH= 6.5, AFR= 2.15 L/min). After a further increase in the RT (up to 12 h), the removal efficiency of phenol, COD, and ammonia increased only slightly to 96.8, 79.2, and 98 %, respectively. A long RT helps in the acclimatization of microorganisms in the wastewater and hence results in improved removal efficiency of the pollutants.

The removal efficiency of phenol, COD, and ammonia also depends on the AFR (Barwal and Chaudhary, 2017; El-Naas et al., 2010). The effect of AFR on the removal of phenol, COD, and ammonia has been shown in the surface and contour plots of Figure 4.12. The removal efficiency increased when the AFR was increased from 0.8 to 2.15 L/min. However, beyond this flow rate (greater than 2.15 LPM), no further improvement in the removal efficiency was obtained. The initial improvement in the removal efficiency due to an increase in the AFR was attributed to the improvement in mixing/contact between the microorganisms and the substrate. This mixing effect became negligible and the RE was not increased too much (only 1% increment) when the AFR was increased beyond a critical limit. So, AFR of 2.15 LPM was found to be an optimum condition for pollutants removal.

**Table 4.8.** Experimentally obtained responses at various conditions used in RSM optimization

| Run | Factor 1<br>*A*:pH | Factor 2<br>*B*:RT<br>h | Factor 3<br>*C*:AFR<br>LPM | Response 1<br>Phenol removal (%) | Response 2<br>COD removal (%) | Response 3<br>Ammonia removal (%) |
|---|---|---|---|---|---|---|
| 1 | 6.5 | 12 | 2.15 | 96.8 | 79.22 | 98.07 |
| 2 | 8 | 12 | 0.8 | 68.72 | 69.24 | 83.22 |
| 3 | 6.5 | 7 | 2.15 | 92.23 | 72.19 | 91.28 |
| 4 | 6.5 | 7 | 3.5 | 93.37 | 73.36 | 95.39 |
| 5 | 6.5 | 7 | 2.15 | 92.0 | 72.24 | 92.22 |
| 6 | 5 | 7 | 2.15 | 61.73 | 52.03 | 56.61 |
| 7 | 5 | 2 | 0.8 | 34.47 | 33.4 | 39.56 |
| 8 | 6.5 | 7 | 2.15 | 91.56 | 72.97 | 90.52 |
| 9 | 8 | 12 | 3.5 | 76.31 | 75.24 | 89.34 |
| 10 | 5 | 2 | 3.5 | 44.12 | 34.64 | 44.21 |
| 11 | 6.5 | 7 | 2.15 | 92.68 | 72.3 | 91.88 |
| 12 | 8 | 2 | 3.5 | 46.35 | 35.62 | 47.59 |
| 13 | 8 | 2 | 0.8 | 40.34 | 32.8 | 41.64 |
| 14 | 6.5 | 2 | 2.15 | 61.21 | 53.64 | 52.66 |
| 15 | 6.5 | 7 | 0.8 | 86.45 | 69.86 | 72.25 |
| 16 | 6.5 | 7 | 2.15 | 92.58 | 72.88 | 91.26 |
| 17 | 6.5 | 7 | 2.15 | 92.56 | 73.13 | 92.59 |
| 18 | 5 | 12 | 0.8 | 63.67 | 59.45 | 65.04 |
| 19 | 5 | 12 | 3.5 | 65.89 | 66.28 | 71.06 |
| 20 | 8 | 7 | 2.15 | 62.2 | 65.28 | 69.21 |

**Table 4.9.** Analysis of fit summary statistics obtained from RSM

| Response | Source | *P*-value | $R^2$ | Adj. $R^2$ | Pred. $R^2$ | Press | SD | CV |
|---|---|---|---|---|---|---|---|---|
| Phenol | Quadratic | <0.0001 | 0.989 | 0.98 | 0.915 | 685.48 | 2.91 | 4.0 |
| COD | Quadratic | <0.0001 | 0.984 | 0.969 | 0.877 | 569.86 | 2.73 | 4.44 |
| Ammonia | Quadratic | <0.0001 | 0.952 | 0.909 | 0.720 | 2209.46 | 6.15 | 8.34 |

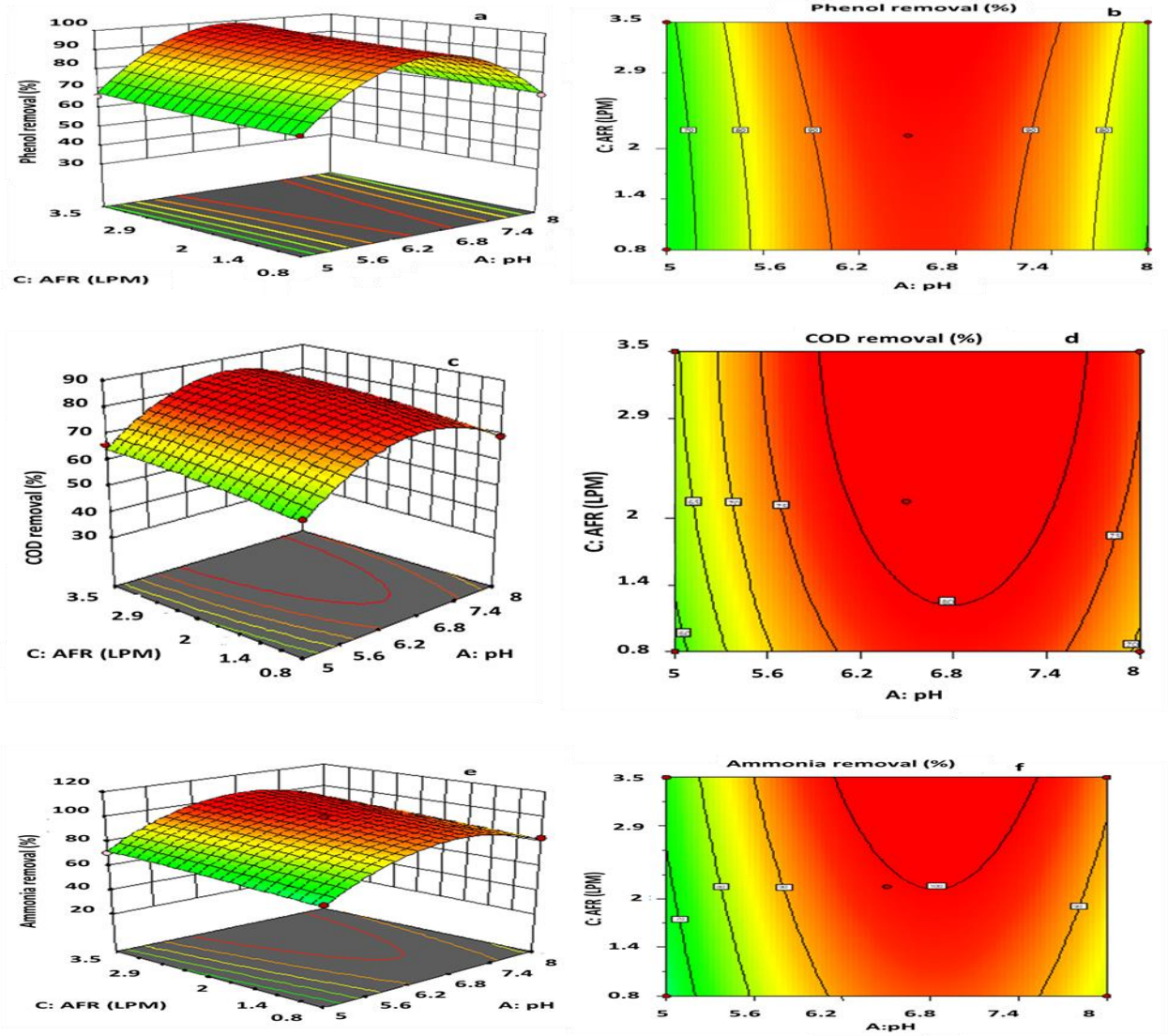


**Figure 4.12.** The effect of simultaneous variation of AFR and pH on the removal of (a, b) phenol; (c, d) COD; (e, f) ammonia.

### 4.6.2.3. Development of correlations for the response variables using ANOVA and CCD model

ANOVA analysis was carried out in order to test the efficacy of the model for phenol, COD, and ammonia removal. The quadratic relationships between the independent variables (pH, RT, and AFR with the parametric symbols *A*, *B*, and *C* respectively) and process responses (phenol, COD, and ammonia removal) were represented in the form of coded equations (Eq. 35-37).

$$\text{Phenol removal (\%)} = +91.0 + 2.4A + 14.4B + 3.2C + 0.92AB + 0.21AC - 0.73BC - 27.19A^2 - 10.15B^2 + 0.75C^2 \quad (35)$$

$$\text{COD removal (\%)} = +72.2 + 3.24A + 15.93B + 2.74C + 2.30AB + 0.0937AC + 1.10BC - 12.92A^2 - 5.14B^2 - 3.46C^2 \quad (36)$$

$$\text{Ammonia removal (\%)} = +88.52 + 5.45A + 18.11B + 4.59C + 3.87AB + 0.175AC + 0.19BC - 20.95A^2 - 8.49B^2 - 0.036C^2 \quad (37)$$

The coded equations help to predict the responses for given levels of each factor during the removal of phenol, COD, and ammonia. The summary of ANOVA analysis for the quadratic model is given in Table 4.10. Again, the high values of *F* and low values of *p* indicated that the quadratic model was suitable for the obtained data.

**Table 4.10.** ANOVA analysis for the quadratic model fitted to various responses

| Response 1: Phenol removal | | | | | |
|---|---|---|---|---|---|
| Source | Sum of squares | *Df* | Mean square | *F* value | *p*-value |
| Model | 7972.71 | 9 | 885.86 | 104.35 | <0.0001 |
| *A*-pH | 57.79 | 1 | 57.79 | 6.81 | 0.0261 |
| *B*-RT | 2099.60 | 1 | 2099.60 | 247.32 | <0.0001 |
| *C*-AFR | 104.91 | 1 | 104.91 | 12.36 | 0.0056 |
| Residual | 84.89 | 10 | 8.49 | | |
| Lack of fit | 83.36 | 5 | 16.67 | 54.48 | 0.0002 |
| Pure error | 1.53 | 5 | 0.3060 | | |
| Cor Total | 8009.61 | 19 | | | |
| Response 2: COD removal | | | | | |
| Source | Sum of squares | *df* | Mean square | *F* value | *p*-value |
| Model | 4570.69 | 9 | 507.85 | 68.30 | <0.0001 |
| *A*-pH | 104.85 | 1 | 104.85 | 14.10 | 0.0038 |
| *B*-RT | 2538.6 | 1 | 2538.6 | 341.42 | <0.0001 |
| *C*-AFR | 75.02 | 1 | 75.02 | 10.09 | 0.0099 |
| Residual | 74.35 | 10 | 7.44 | | |
| Lack of fit | 73.47 | 5 | 14.69 | 83.31 | <0.0001 |
| Pure error | 0.8819 | 5 | 0.1764 | | |
| Cor Total | 4645.05 | 19 | | | |
| Response 3: Ammonia removal | | | | | |
| Source | Sum of squares | *df* | Mean square | *F* value | *p*-value |
| Model | 7535.31 | 9 | 837.25 | 22.11 | <0.0001 |
| *A*-pH | 297.24 | 1 | 297.24 | 7.85 | 0.0187 |

| | | | | | |
|---|---|---|---|---|---|
| *B*-RT | 3278.63 | 1 | 3278.63 | 86.58 | <0.0001 |
| *C*-AFR | 210.5 | 1 | 210.5 | 5.56 | 0.0401 |
| Residual | 380.26 | 10 | 38.03 | | |
| Lack of fit | 378.66 | 5 | 75.17 | 133.11 | <0.0001 |
| Pure error | 2.82 | 5 | 0.5647 | | |
| Cor Total | 7913.88 | 19 | | | |

#### 4.6.2.4. Verification of the developed model

The CCD of RSM was applied to minimize the retention time (RT) and airflow rate (AFR) in the desired pH range of 5.0 – 8.0 for the maximum removal of phenol, COD, and ammonia. The software predicted a set of experiments by the numerical method to obtain maximum removal efficiency with minimal input. The optimum process conditions were observed to be pH of 6.5, RT of 7.0 h, and AFR of 2.15 L/min with 91.2, 72.4, and 88.7 % removal efficiency of phenol, COD, and ammonia removal, respectively with the desirability of 0.93. The set of experiments was performed at optimized process conditions, and the obtained results were compared with the predicted data. The removal percentage of phenol, COD, and ammonia were obtained as 92.23 ± 0.4, 72.57 ± 0.4, and 90.49 ± 0.3 %, respectively, from the experiments. Apparently, the errors between the predicted and obtained removal efficiency of phenol, COD, and ammonia were within the range of 5%, which endorsed the reliability of the values obtained from the statistical model developed in this study.

### 4.6.3. Kinetic study

#### 4.6.3.1. First-order kinetic model

The kinetic constants were evaluated from the straight-line graph plotted between $\frac{S_0-S}{t}$ against the concentration ($S$) (Figure 4.13). The lumped first-order kinetic constants ($k_1$) for phenol, COD, and ammonia were obtained as 0.868, 0.52, and 0.65 $h^{-1}$, respectively. The corresponding first-order rate constants were calculated form Eq. (21) and resulted of 0.27, 0.16, and 0.20 L/gVSS. h. The values of the coefficient of determination ($R^2$) were obtained as 0.964, 0.926, and 0.916 for phenol, COD, and ammonia removal, respectively using the first-order kinetic.

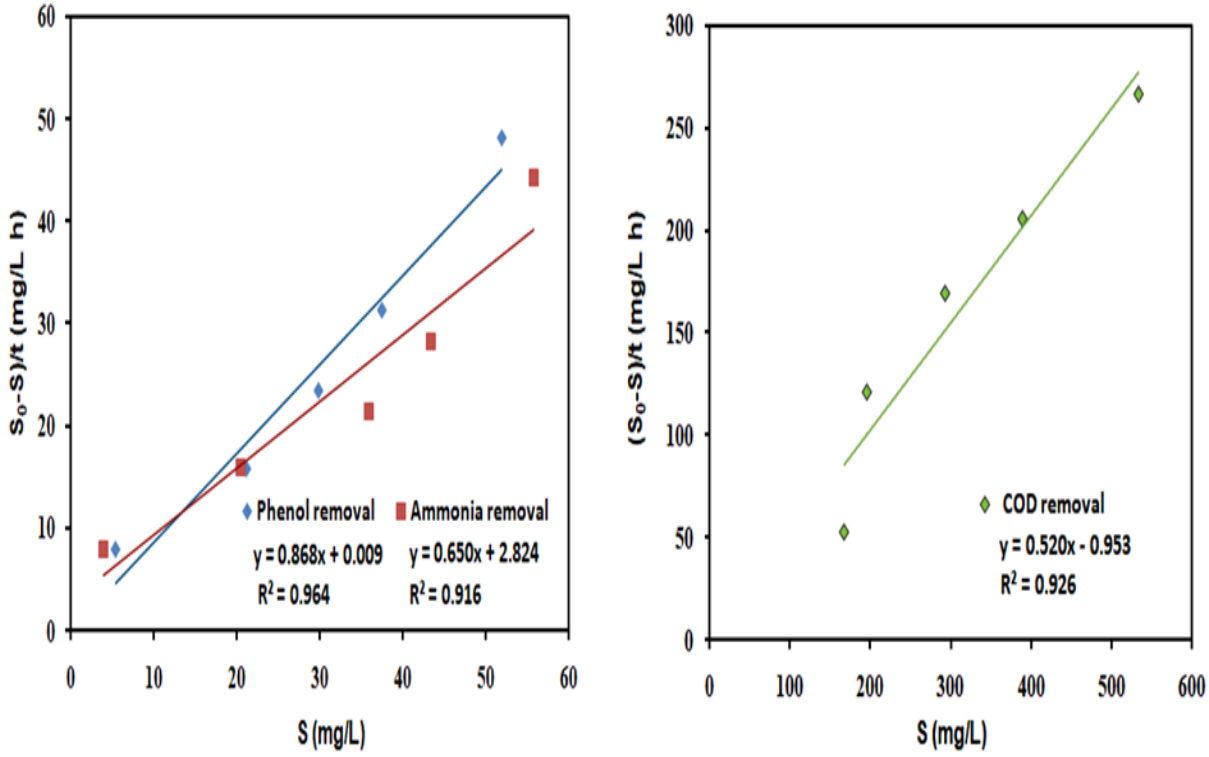


**Figure 4.13.** First-order kinetic model plot for the removal of phenol, ammonia, and COD.

#### 4.6.3.2. Second-order kinetic model

The graphical representation of *t/E* against *E* for phenol, COD, and ammonia based on the second-order equation was provided in Figure 4.14. The kinetic parameters such as *n* and *m* were evaluated from the slopes and intercepts obtained from the graphs. The kinetic

parameter *n* was obtained of 0.955, 1.117, and 0.908 for phenol, COD, and ammonia, respectively. Similarly, another kinetic parameter *m* was obtained of 1.311, 1.536, and 1.671 h, respectively. The values of second-order rate constants ($k_s$) were evaluated from Eq. (23) and obtained of 2.35, 0.25, and 1.85 $L^2$/ gVSS. gCOD. h for phenol, COD, and ammonia, respectively. The value of the second-order rate constant depends on the concentration of pollutants and the biomass in the bioreactor. The summary of kinetic parameters obtained from first-order and second-order kinetic models was represented in Table 4.11. The correlation coefficients ($R^2$) for phenol, COD, ammonia were above 0.99, which indicated that the second-order kinetic model had better predictability than the first-order model. The kinetic model presented in this study can be used in the design calculations of a MBBR for the collective removal of phenol and ammonia.

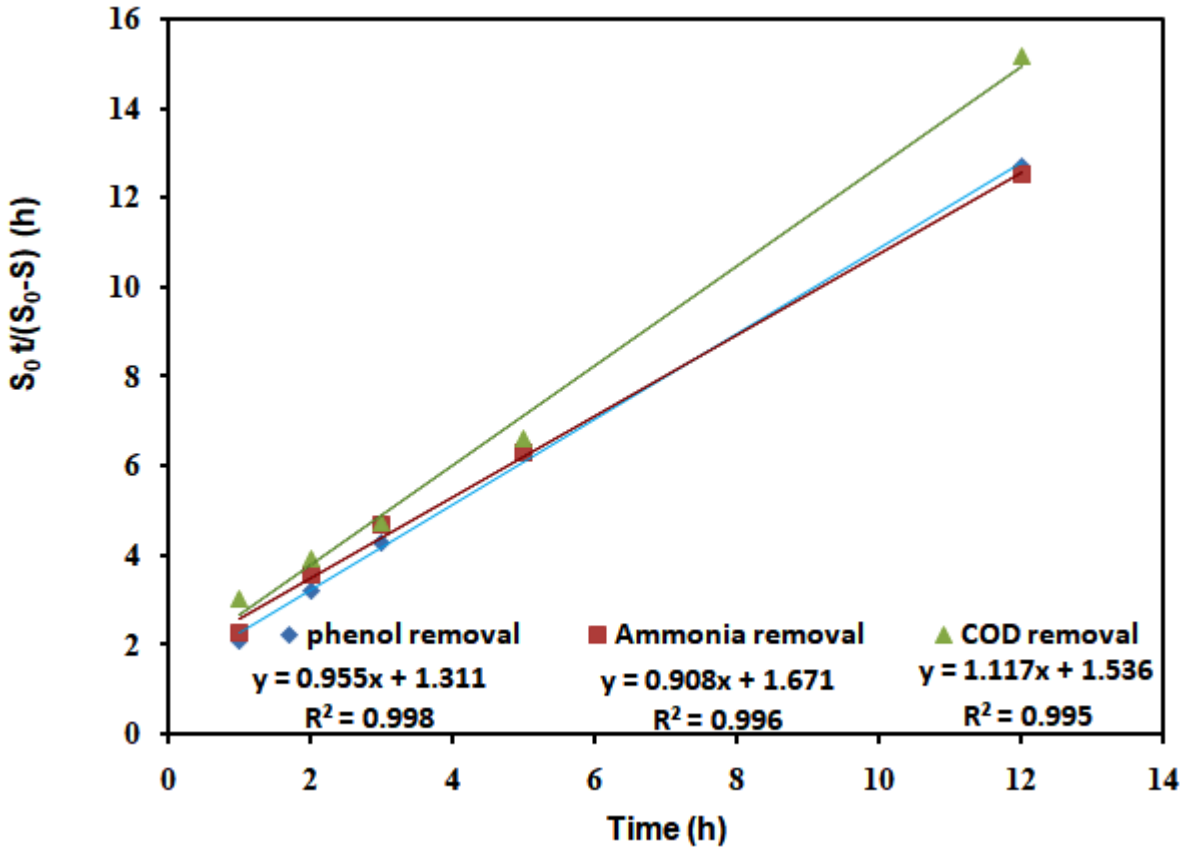


**Figure 4.14.** Second-order kinetic model plot for the removal of phenol, ammonia, and COD.

**Table 4.11.** Summary of kinetic parameters obtained by first-order and second-order model for removal of phenol, COD, and ammonia, respectively.

| Model | First-order | | Second-order | | | |
|---|---|---|---|---|---|---|
| | $k$ (L/g VSS. h) | $R^2$ | $n$ | $m$ (h) | $k_s$ ($L^2$/gVSS. gCOD.h) | $R^2$ |
| phenol | 0.868 | 0.964 | 0.955 | 1.311 | 2.35 | 0.998 |
| COD | 0.520 | 0.926 | 1.117 | 1.536 | 0.25 | 0.995 |
| Ammonia | 0.650 | 0.916 | 0.908 | 1.671 | 1.85 | 0.996 |

### 4.7. Phytotoxicity analysis

A phytotoxicity test was done over 7.0 days using *Vigna Radiata* seeds at laboratory conditions (28 ± 2.0 °C). The control experiment was carried out in distilled water and the germination images were represented in Figure 4.15. It was found that the toxic effect of phenol causes lower germination and higher phytotoxicity (%) compared to the treated wastewater. The germination (%) values were found to be 73 and 86 % for untreated and treated wastewater, respectively (Table 4.12). After the biodegradation of phenol, the toxic effect was significantly reduced, which induced higher growth of plumules and radicles. Further, the growth of radicles were measured to be 4.50 and 5.63 cm for untreated and treated wastewater, respectively. Previously, Wolski et al., 2012 have evaluated wheat germination during biodegradation of phenol (initial phenol concentration of 400 mg/L). They found that the germination was improved from 6.25 % to 95 % after the mineralization of phenol wastewater.


**Figure 4.15.** Images of *Vigna radiata* seeds germinated in (a) distilled water, (b) untreated wastewater, (c) treated wastewater.

**Table 4.12.** A summary of toxicity analysis of treated and untreated wastewater by *Vigna radiata* seed germination.

| S.N. | Parameters | Unit | Distilled water | Untreated wastewater | Treated wastewater |
|---|---|---|---|---|---|
| 1 | Germination | (%) | 100 ± 0 | 73 ± 1.35 | 86 ± 1.57 |
| 2 | Phytotoxicity | (%) | - | 26.2 ± 1.68 | 7.7 ± 1.03 |
| 3 | Radicle length | cm | 6.10 ± 1.85 | 4.50 ± 2.15 | 5.63 ± 2.23 |
| 4 | Plumule length | cm | 5.40 ± 1.04 | 3.21 ± 1.48 | 5.33 ± 1.94 |

### 4.8. Analysis of metabolites during biodegradation of phenol

The GC-MS analysis of the samples was done to detect the metabolites formed during the biodegradation of phenol and shown in Figure 4.16 (a, b). The peak of untreated wastewater

containing phenol (control) showed a peak at a retention time of 7.80 min (Figure 4.16a) whereas, several peaks were observed in the case of the treated wastewater. However, two major metabolites such as catechol (17.89 min) and 2-hydroxymuconic semialdehyde (22.48 min) were detected during the biodegradation of phenol (Figure 4.16b). In addition, the GC-MS fragmentation patterns on the basis of mass/charge of the metabolites were represented in Figure 4.17. In aerobic conditions, the bacterial sp. degrade phenol into catechol in the presence of phenol hydroxylase enzyme (Lakshmi and Sridevi, 2015). In the meta-cleavage pathway, catechol is again metabolized to form 2-hydroxymuconic semialdehyde, which is successively further degraded to form pyruvate and acetaldehyde. Previously, Nie et al., 2016 reported that catechol and 2-hydroxymuconic semialdehyde were the major metabolites detected during the biodegradation of phenol by *Pseudomonas stutzeri* N2.

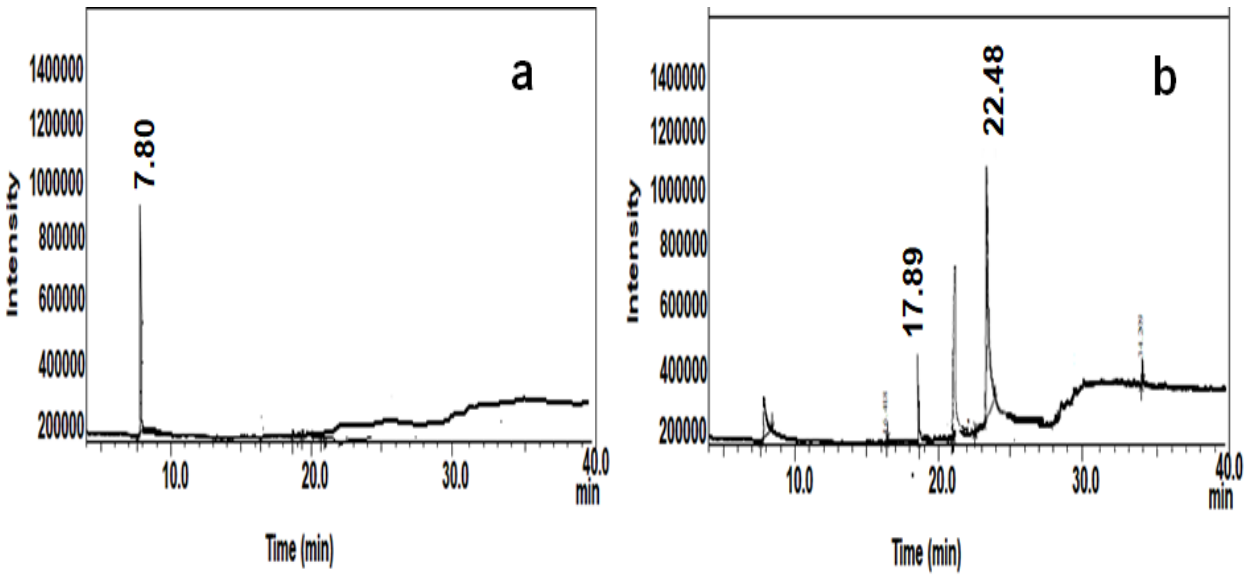


**Figure 4.16.** GC-MS analysis of (a) phenol (control); (b) treated wastewater.

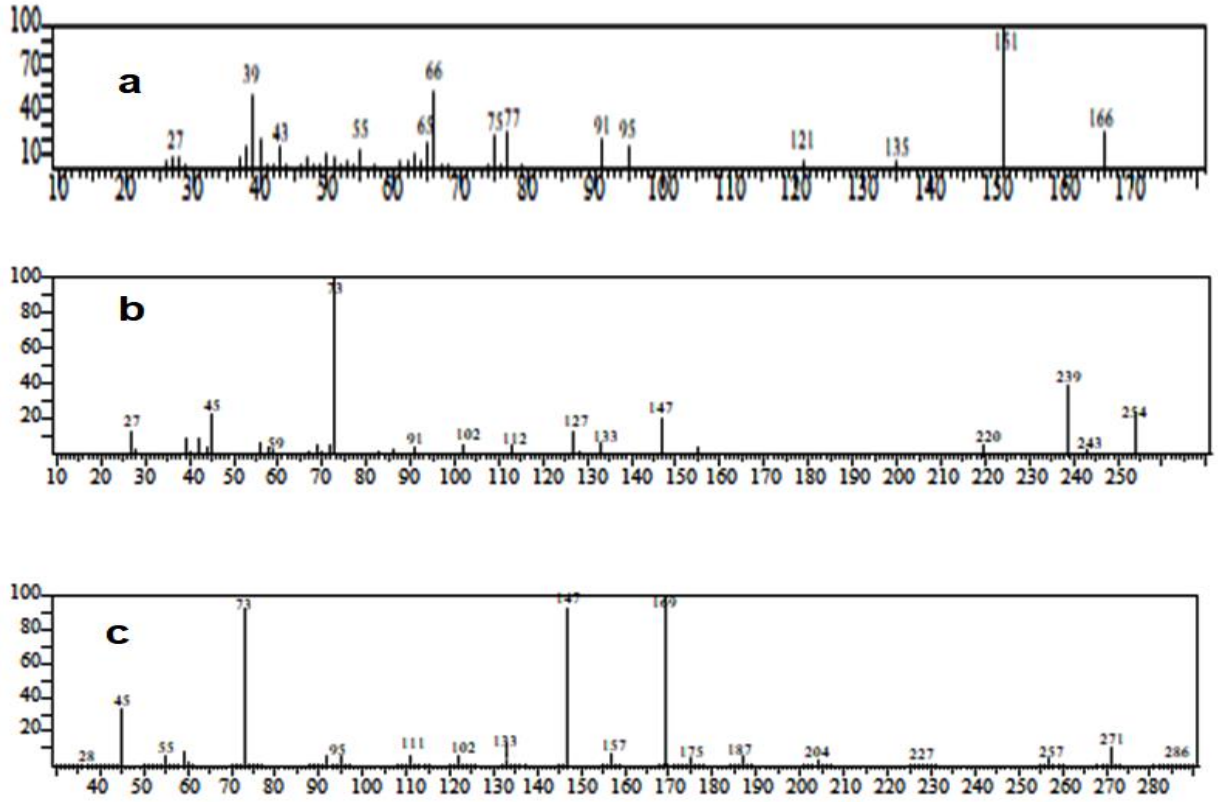


**Figure 4.17.** GC-MS spectra of control (a) phenol and intermediate metabolites (b) catechol and (c) 2-hydroxymuconic semialdehyde.

## Section B: 4-chlorophenol biodegradation

### 4.9. Optimization study

The process parameters such as 4-chlorophenol (4-CP) concentration (40 – 100 mg/L), peptone concentration (0 – 0.6 g/L), and hydraulic retention time (HRT) (8 – 36 h) were optimized using CCD of RSM for the biodegradation of 4-CP. The obtained responses are summarized in Table 4.13. The correlation developed between the independent process variables and the response (4-CP and COD removal %) has been expressed in the form of a second-order polynomial equation as:

4-CP removal (%) = 76.69 - 4.04 $A$ + 7.44 $B$ + 24.14 $C$ + 0.3275 $AB$ + 1.67 $AC$ + 3.31 $BC$ – 3.25$A^2$–2.13$B^2$– 14.14 $C^2$ (38)

COD removal (%) = 66.49 - 4.29 $A$ + 6.87 $B$ + 23.62 $C$ - 0.38 $AB$ + 1.38 $AC$ + 3.55 $BC$ – 3.61 $A^2$–2.09 $B^2$ – 14.86 $C^2$ (39)

The values of $R^2$, adjusted $R^2$, and predicted $R^2$ were obtained to be 0.996, 0.993, and 0.979, respectively, for 4-CP removal. Similarly, corresponding regression coefficients were obtained to be 0.988, 0.979, and 0.903, respectively, for COD removal. The obtained value of $R^2$ is greater than 0.8, which represents that the quadratic model was in reasonable agreement with the experimental data. The obtained $p$ values for 4-CP concentration, peptone concentration, and HRT were less than 0.05, representing the important role of the process parameters in the model (Table 4.14). Moreover, ANOVA analysis was carried out to analyze the consistency of the model (Table 4.15). The higher value of $f$ and the lower value of $p$ (< 0.05) shows that the parameters are more significant.

**Table 4.13.** Experimentally obtained responses at various conditions used in RSM optimization

| Run | Factor 1 *A*:4-CP concentration (mg/L) | Factor 2 *B*: Peptone concentration (g/L) | Factor 3 *C*: HRT (h) | Response 1 4-CP removal (%) | Response 2 COD removal (%) |
|---|---|---|---|---|---|
| 1 | 70 | 0.3 | 22 | 75.16 ± 2.67 | 63.28 ± 3.60 |
| 2 | 100 | 0 | 8 | 23.09 ± 1.04 | 16.47 ± 2.01 |
| 3 | 70 | 0.3 | 22 | 76.04 ± 3.19 | 65.93 ± 1.53 |
| 4 | 40 | 0.3 | 22 | 77.46 ± 2.48 | 67.07 ± 2.42 |
| 5 | 70 | 0.3 | 8 | 36.68 ± 1.77 | 23.11 ± 2.03 |
| 6 | 70 | 0.3 | 22 | 76.39 ± 3.05 | 68.62 ± 3.36 |

| | | | | | |
|---|---|---|---|---|---|
| 7 | 70 | 0.6 | 22 | 81.90 ± 3.25 | 70.28 ± 2.53 |
| 8 | 100 | 0 | 36 | 66.51 ± 2.82 | 54.39 ± 2.26 |
| 9 | 100 | 0.6 | 8 | 32.06 ± 1.58 | 19.72 ± 3.11 |
| 10 | 70 | 0.3 | 36 | 89.84 ± 1.17 | 78.95 ± 1.85 |
| 11 | 100 | 0.6 | 36 | 89.42 ± 2.79 | 77.51 ± 2.43 |
| 12 | 70 | 0.3 | 22 | 76.18 ± 3.47 | 66.3 ± 1.80 |
| 13 | 40 | 0.6 | 8 | 43.52 ± 2.83 | 34.2 ± 3.47 |
| 14 | 40 | 0 | 36 | 72.61 ± 2.79 | 61.81 ± 2.62 |
| 15 | 40 | 0.6 | 36 | 93.53 ± 3.94 | 80.79 ± 1.49 |
| 16 | 40 | 0 | 8 | 35.18 ± 3.49 | 23.77 ± 1.74 |
| 17 | 100 | 0.3 | 22 | 70.84 ± 2.91 | 57.49 ± 2.73 |
| 18 | 70 | 0 | 22 | 68.64 ± 1.20 | 57.32 ± 1.40 |
| 19 | 70 | 0.3 | 22 | 78.20 ± 2.36 | 69.14 ± 2.53 |
| 20 | 70 | 0.3 | 22 | 75.34 ± 2.93 | 68.07 ± 3.26 |

RSM: Response surface methodology; 4-CP: 4-chlorophenol; HRT: Hydraulic retention time; COD: Chemical oxygen demand.

### 4.10. Simultaneous effect of process parameters on 4-CP and COD removal

#### 4.10.1. Effect of 4-CP concentration and peptone concentration

The interactive impact of 4-CP concentration and peptone concentration on 4-CP and COD removal (%) was depicted by three-dimensional and surface contour plots (Figure 4.18 (a, b) and Figure 4.19 (a, b)). The 4-CP and COD removal of 77.06 and 67.07 %, respectively were achieved at an initial 4-CP concentration of 40 mg/L (peptone concentration = 0.3 g/L; HRT = 22 h). However, by increasing the 4-CP concentration up to 100 mg/L, the removal was decreased to 70.84 and 57.49 %, respectively, for 4-CP and COD at similar operating conditions (Table 4.13). The attached biomass could be able to remove a specific amount of pollutants in a certain time period. At a higher concentration, more time will be required for

the complete mineralization of the pollutant. The peptone acts as a nitrogenous source which is responsible for the formation of protein and nucleic acid in microorganisms. The high growth of biomass was observed due to the presence of peptone, which helps in better removal efficiency. The 4-CP removal was improved from 68.64 to 81.9 % with increasing the peptone concentration from 0 to 0.6 g/L (4-CP concentration = 70 mg/L, HRT = 22 h). In the meantime, the total biomass was increased from 1430 mg/L to 1595 mg/L with peptone concentration (data not shown).

### 4.10.2. Effect of HRT and peptone concentration

Figure 4.18 (b, c) and Figure 4.19 (b, c) represent the effect of HRT and peptone concentration on the removal of 4-CP and COD, respectively. HRT has a significant impact on the biodegradation of organic pollutants. The removal of 4-CP was obtained to be 36.68 and 89.84 % at HRT of 8 and 36 h, respectively, at a constant 4-CP and peptone concentration. Similarly, COD removal was also improved and evaluated to be 63.28 and 78.95 %, respectively, under similar operating conditions. In addition, a slight increment of biomass has been observed with the increase of HRT. The corresponding biomass was found to be 1487 and 1573 mg/L, respectively. The low HRT induces insufficient contact time between the bacterial site and the pollutant molecules, resulting in incomplete mineralization of 4-CP. With the increase of peptone concentration from 0.3 to 0.6 g/L, a slight increase in 4-CP and COD removal was observed. The maximum removal of 78.2 and 81.9 % of 4-CP removal was observed (4-CP concentration = 70 mg/L; HRT = 22 h). Moreover, COD removals of 69.14 and 70.28 % were found at similar conditions.

### 4.10.3. Effect of 4-CP concentration and HRT

The effect of the initial 4-CP concentration and HRT on 4-CP and COD removal was shown in Figure 4.18 (e, f) and Figure 4.19 (e, f), respectively. At a constant HRT and

peptone concentration, the MBBR was able to remove 43.52 and 32.06 % of 4-CP when the 4-CP concentration was increased from 40 to 100 mg/L. However, the amount of 4-CP removed was higher in the case of 100 mg/L (32.06 mg/L) compared to the 40 mg/L (17.41 mg/L). This was due to the increase of substrate (4-CP) concentration gradient along the column, which enhanced the availability of more 4-CP. Similarly, COD removal was also decreased from 34.2 to 19.72 % due to the presence of residual 4-CP and intermediate products. It was observed that the MBBR performance was reduced at lower HRT conditions. Hence, the bioreactor should be operated at a higher HRT value to obtain maximum removal of 4-CP and COD.

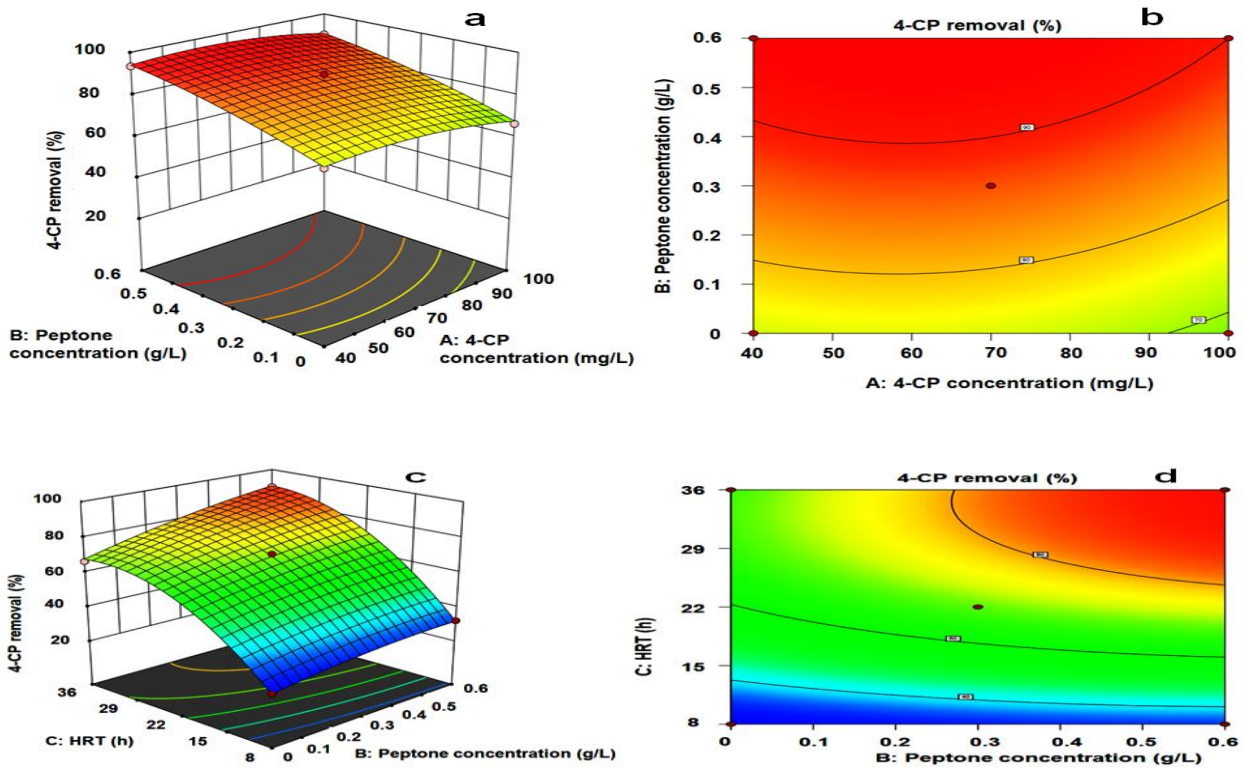

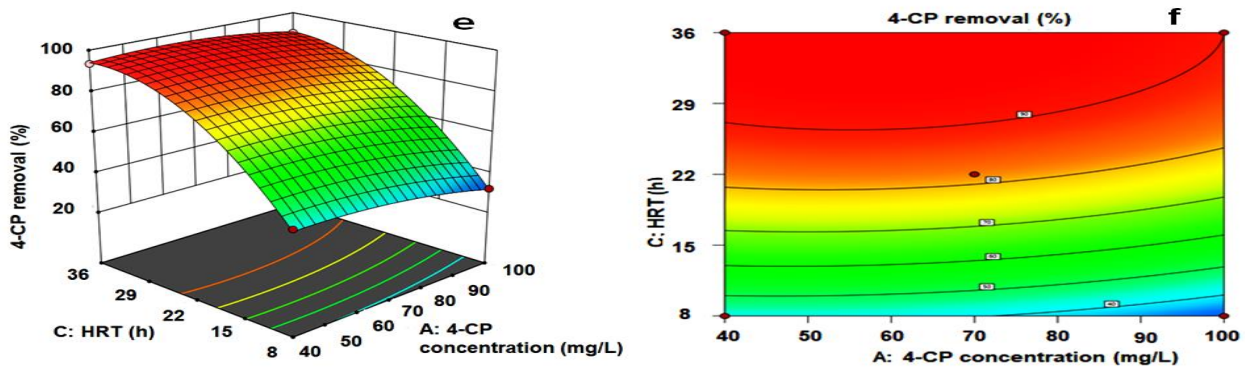


**Figure 4.18.** The response surface methodology plots for the biodegradation of 4-CP: (a, b) effect of peptone and 4-CP concentration; (c, d) effect of HRT and peptone concentration; (e, f) effect of HRT and 4-CP concentration.

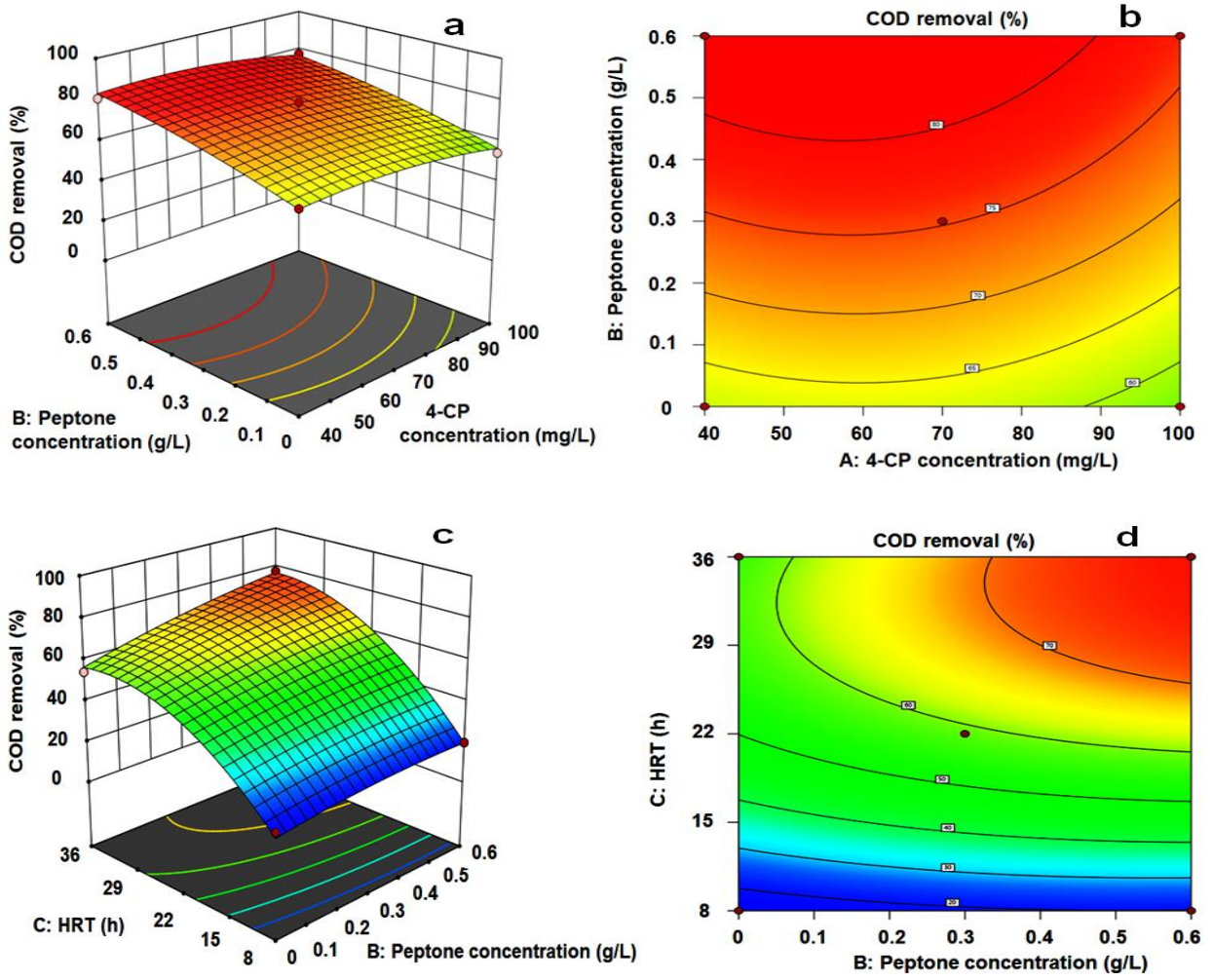

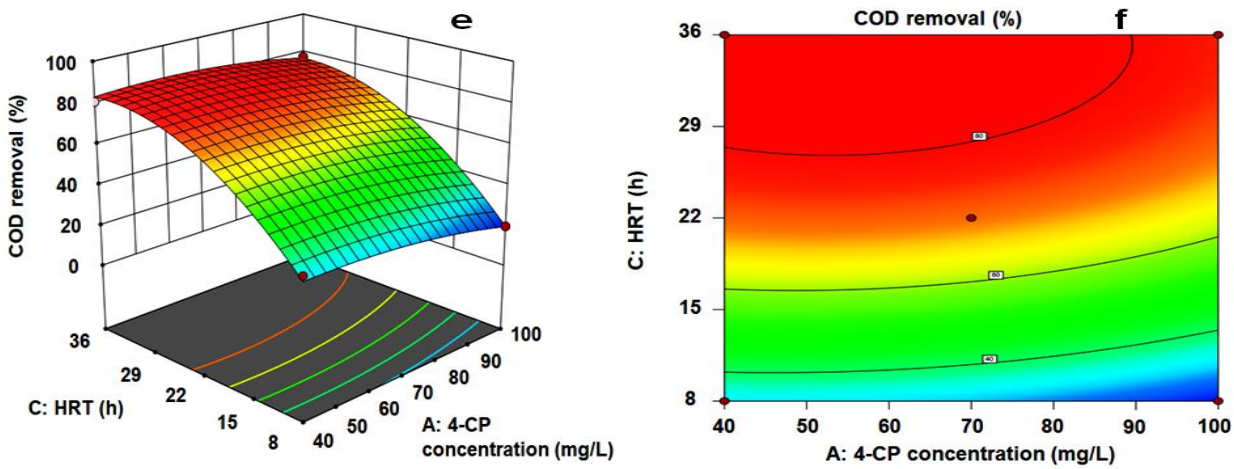


**Figure 4.19.** The response surface methodology plots for the biodegradation of COD: (a, b) effect of peptone and 4-CP concentration; (c, d) effect of HRT and peptone concentration; (e, f) effect of HRT and 4-CP concentration.

**Table 4.14.** Analysis of fit summary statistics obtained from RSM

| Response | Source | *P*-value | $R^2$ | Adj. $R^2$ | Pred. $R^2$ | SD | CV |
|---|---|---|---|---|---|---|---|
| 4-CP | Quadratic | <0.0001 | 0.996 | 0.993 | 0.979 | 1.69 | 2.53 |
| COD | Quadratic | <0.0001 | 0.988 | 0.979 | 0.903 | 3.01 | 5.35 |

**Table 4.15**. ANOVA analysis for the quadratic model fitted to various responses

| Response 1: 4-CP removal | | | | | |
|---|---|---|---|---|---|
| Source | Sum of squares | *df* | Mean square | *F* value | *p*-value |
| Model | 8227.79 | 9 | 914.20 | 319.60 | <0.0001 |
| *A*- 4-CP concentration | 163.05 | 1 | 163.05 | 57.00 | <0.0001 |
| *B*- Peptone concentration | 553.54 | 1 | 553.54 | 193.51 | <0.0001 |
| *C*- HRT | 5826.43 | 1 | 5826.43 | 2036.88 | <0.0001 |
| Residual | 28.60 | 10 | 2.86 | | |

| | | | | | |
|---|---|---|---|---|---|
| Lack of fit | 22.72 | 5 | 4.54 | 3.86 | 0.0821 |
| Pure error | 5.88 | 5 | 1.18 | | |
| Response 2: COD removal | | | | | |
| Source | Sum of squares | *df* | Mean square | *F* value | *p*-value |
| Model | 8089.15 | 9 | 898.79 | 99.22 | <0.0001 |
| *A*-4-CP concentration | 176.9 | 1 | 176.9 | 19.53 | 0.0013 |
| *B*- Peptone concentration HRT | 472.52 | 1 | 472.52 | 52.16 | <0.0001 |
| *C*-HRT | 5578.1 | 1 | 5578.1 | 615.81 | <0.0001 |
| Residual | 90.58 | 10 | 9.06 | | |
| Lack of fit | 66.83 | 5 | 13.37 | 2.81 | 0.1403 |
| Pure error | 23.75 | 5 | 4.75 | | |

ANOVA: Analysis of variance; HRT: Hydraulic retention time; COD: Chemical oxygen demand.

**4.10.4. Verification of the developed model**

The optimization of the quadratic model was performed by selecting the maximum concentration of the pollutant, HRT, and a desirable range of peptone concentration to obtain maximum removal of 4-CP and COD. The corresponding optimum values of the process parameters were obtained to be 100 mg/L, 36 h, and 0.6 g/L. The responses were predicted to be 89.97 and 76.79 % of 4-CP and COD removal with a desirability of 0.97. To validate the model, the MBBR was operated at the optimized process conditions of 4-CP concentration, HRT, and peptone concentration. The responses were obtained as 91.07 and 75.29 % for 4-CP and COD removals, respectively. The obtained values of the responses were within the range of ± 2.0 %, which implies that the above model would suitably predict the experimental value.

### 4.11. Kinetic analysis

#### 4.11.1. Monod model

The growth rate of bacterial species was studied using the Monod model and graphs were plotted between $\frac{t.X}{F_0-F}$ and $\frac{1}{F}$ (Figure 4.20). The values of $k_s$ and $k$ were evaluated from the graph and obtained as 20.68 mg/L and 0.107 $d^{-1}$ for 4-CP. Similarly, the corresponding kinetic parameters for COD removal were evaluated to be 183 mg/L and 0.368 $d^{-1}$. The regression coefficients were found to be 0.96 and 0.94 for 4-CP and COD removal, respectively. Ahmadi et al. (2017) have applied the Monod model to analyze the bacterial growth in the MBBR during the biodegradation phenol at a concentration of 500 mg/L. The kinetic parameters were evaluated to be 130.32 mg/L for $k_s$ and 16.47 $d^{-1}$ for $k$.

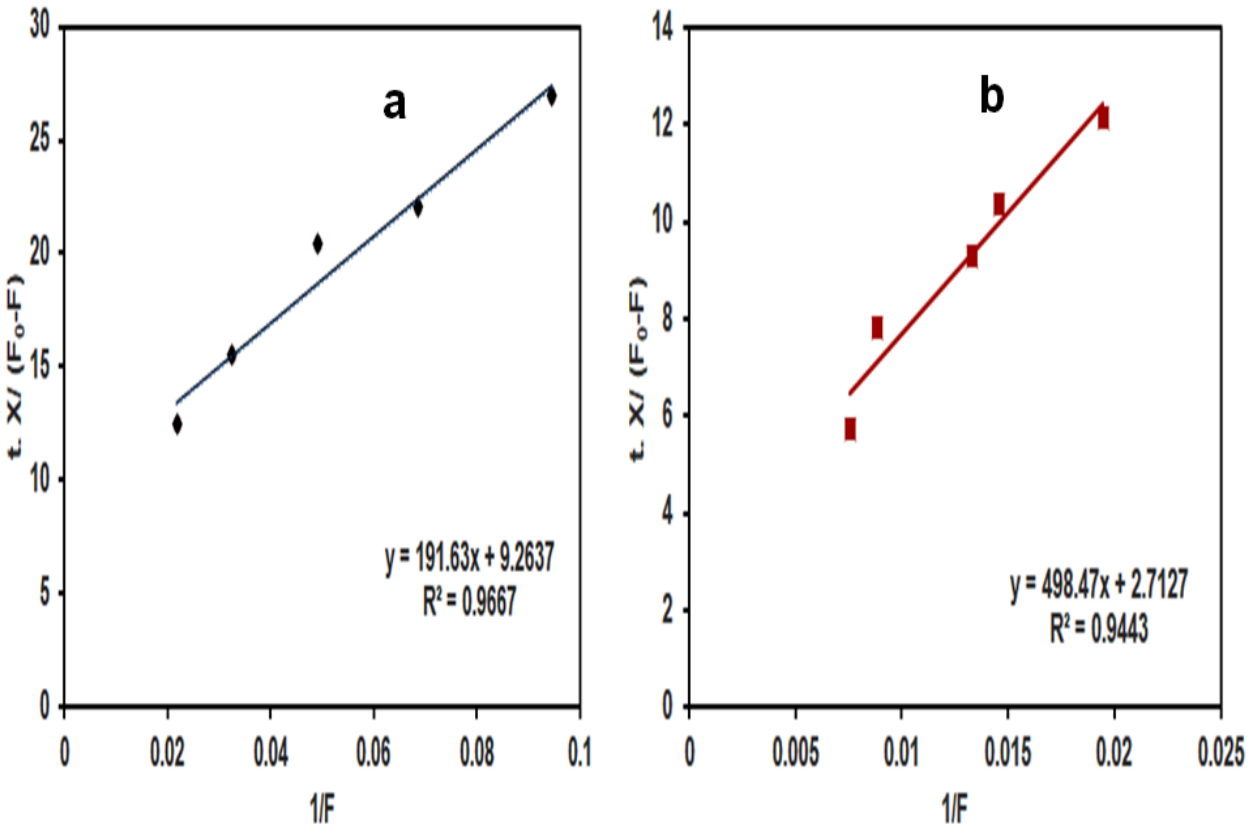


**Figure 4.20.** Monod model plot for the removal of (a) 4-CP, (b) COD.

### 4.11.2. Modified Stover-Kincannon model

The linear plots between $\frac{V}{(F_0-F).\ Q}$ and $\frac{V}{Q.\ F_0}$ have been shown in Figure 4.21 and the summary of the kinetic parameters obtained from modified the Stover-Kincannon model is given in Table 4.16. The regression coefficients were obtained to be 0.99 and 0.98 for 4-CP and COD removals, respectively. The maximum substrate removal rate constants ($U_{max}$) and saturation constants ($K_B$) were evaluated from the slope and intercepts. The kinetic parameters were obtained as $U_{max}$: 0.641 g/L. d, $K_B$: 0.63 g/L. d for 4-CP removal; $U_{max}$: 0.453 g/L. d, $K_B$: 0.404 g/L. d for COD removal. The kinetic parameters were evaluated to be 5.283 g/L. d for $U_{max}$ and 8.052 g/L. d for $K_B$ during the biodegradation of phenol in a three-stage MBBR (Sahariah and Chakraborty, 2011). Oberoi and Philip (2017) have used the modified Stover-Kincannon model for biodegradation of phenolic compounds in a MBBR using activated sludge. They found that the kinetic coefficients, i.e., $U_{max}$ and $K_B$ were evaluated and found to be 2.68 and 2.68 g/L. d, respectively. The obtained value of kinetic parameters in this study is lower than the other literature due to the variation of microorganisms, reactor configuration, biocarriers, and substrate concentration.

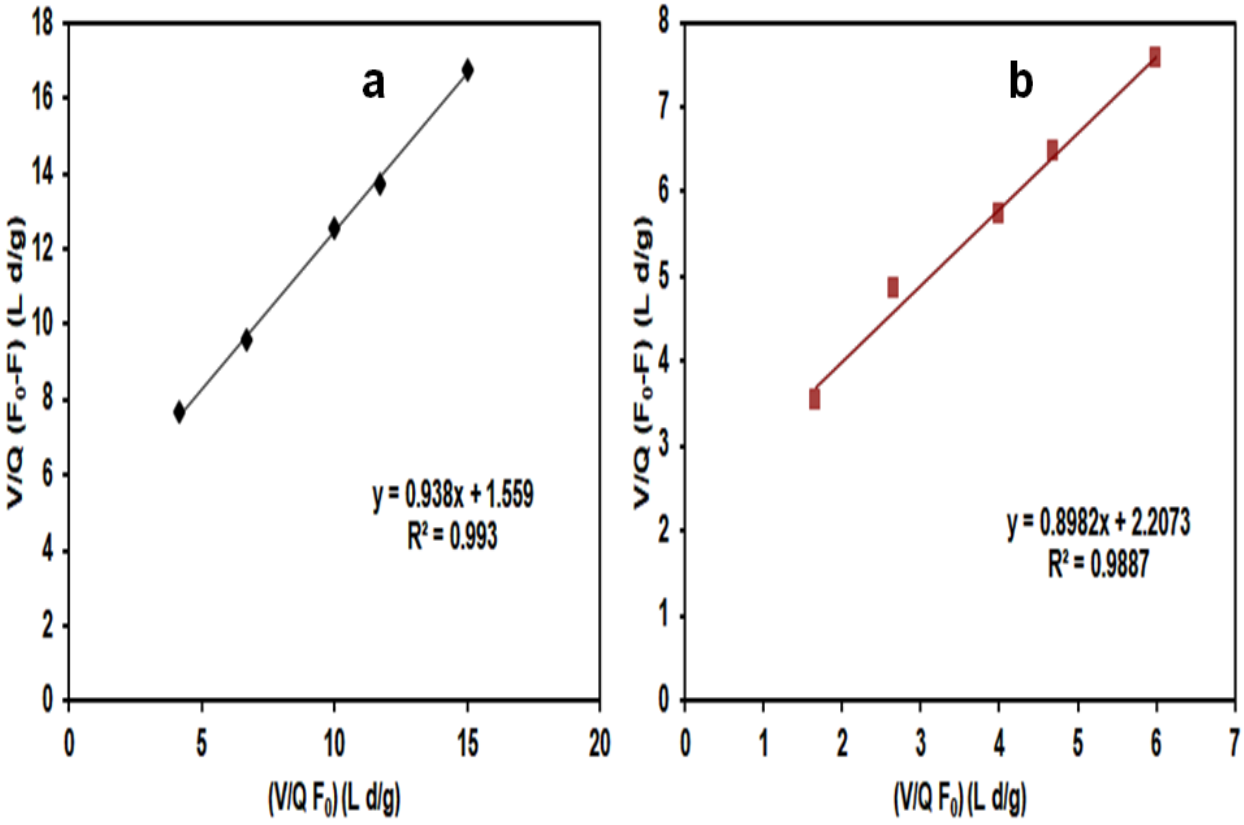


**Figure 4.21.** Modified Stover-Kincannon model plot for the removal of (a) 4-CP, (b) COD.

**Table 4.16.** Summary of kinetic parameters obtained by Monod and modified Stover-Kincannon model for removal of 4-CP and COD, respectively.

| Model | Monod | | | Modified Stover-Kincannon | | |
|---|---|---|---|---|---|---|
| Kinetic parameters | $k$ | $K_s$ | $R^2$ | $U_{max}$ | $K_B$ | $R^2$ |

| | | | | | | |
|---|---|---|---|---|---|---|
| 4-CP | 0.107 | 20.686 | 0.966 | 0.641 | 0.630 | 0.993 |
| COD | 0.368 | 183 | 0.944 | 0.453 | 0.404 | 0.988 |

### 4.12. Phytotoxicity analysis

The phytotoxicity analysis was carried out on Vigna radiata seeds using untreated and treated wastewater. The images of the growth of roots of the seeds in distilled water, untreated wastewater, and treated wastewater have been given in Figure 4.22. The germination (%) was evaluated and found to be 100, 76 ± 1.46, and 84 ± 2.68 % for distilled water, untreated wastewater, and treated wastewater, respectively (Table 4.17). The length of the radicles and plumule were measured after 7.0 days of incubation. The distilled water shows maximum growth of radicle and is obtained to be 5.83 ± 2.24 cm whereas 3.5 ± 2.75 cm of radicle growth was observed for the untreated wastewater. The growth of the radicle was improved after the biodegradation of 4-CP, and the radicle was grown up to 5.26 ± 3.11 cm. For untreated and treated wastewater, the phytotoxicity was measured using Eq. (28) and evaluated to be 39.9 ± 2.60 and 9.6 ± 1.03 %, respectively. In addition, the significant decrease of the toxicity of the wastewater enhances the plumule growth. Hence, the treated wastewater can be used for irrigation purposes.


**Figure 4.22.** Images of *Vigna radiata* seeds germinated in (a) distilled water, (b) untreated wastewater, (c) treated wastewater (after 7.0 days).

**Table 4.17.** A summary of toxicity analysis of treated and untreated wastewater by *Vigna radiata* seed germination.

| S.N. | Parameters | Unit | Distilled water | Untreated wastewater | Treated wastewater |
|---|---|---|---|---|---|
| 1 | Germination | (%) | 100 ± 0 | 76 ± 1.46 | 84 ± 2.68 |
| 2 | Phytotoxicity | (%) | - | 39.9 ± 2.60 | 9.6 ± 1.03 |
| 3 | Radicle length | cm | 5.83 ± 2.24 | 3.5 ± 2.75 | 5.26 ± 3.11 |
| 4 | Plumule length | cm | 5.25 ± 1.18 | 3.17 ± 1.96 | 4.59 ± 2.29 |

**Section C: Comparison of efficiency of a packed bed and a moving bed biofilm reactor**

**4.13. Effect of HRT on the performance of MBBR and PBBR**

After the start-up, the MBBR and PBBR were operated in two stages for 210 days, and the summaries of experimental outcomes are given in Table 4.18 and Table 4.19, respectively. The bioreactors were operated at each operating condition till steady-state performance was achieved. In the first stage, the effect of HRT on the performance of the bioreactors was analysed by operating the bioreactors at 5 different HRTs (48, 36, 24, 16, and 10 h) with 50 mg/L of initial 4-CP concentration (Figure 4.23 (a, b)). The ILR and HRT were set at 0.025 kg/$m^3$.d and 48 h, respectively, after the immobilization of bacterial species on PP-PUF carriers. The maximum REs of 4-CP were obtained as 94.34 and 90.62 % in MBBR and PBBR, respectively. The corresponding COD REs were found to be 83.26 and 79.37 %, respectively, at an HRT of 48 h. When the HRT was decreased from 48 to 36 h, there was a slight change in REs in MBBR and PBBR. The REs of 4-CP and COD were evaluated to be 92.75 and 78.46 %, respectively, in MBBR. Whereas, REs of 4-CP and COD were found to be 81.39 and 70.53 %, respectively, in PBBR. Further, the REs of 4-CP were decreased to 78.61 and 69.16 % for the MBBR and PBBR, respectively, at 24 h. Similarly, the COD REs were found to be 69.97 and 58.76 % for MBBR and PBBR, respectively. At low HRT, the decrease of REs was mainly due to the inadequate contact between the bacterial cells and the pollutant molecules. Sufficient time is required for the effective growth of the bacterial species. Insufficient time causes the decline of extracellular enzymatic activity. Kureel et al., 2018 have evaluated the effect of ILR on the performance of a continuous PBBR for benzene removal. They have reported that the RE of benzene was decreased at a high flow rate or low HRT due to the washout of the substrate without degradation by the bacterial species. Similar kinds of results were also reported in the other literature for the biodegradation of dye and aromatic compounds (Banerjee and Ghoshal; 2016; Kwean et al., 2018).

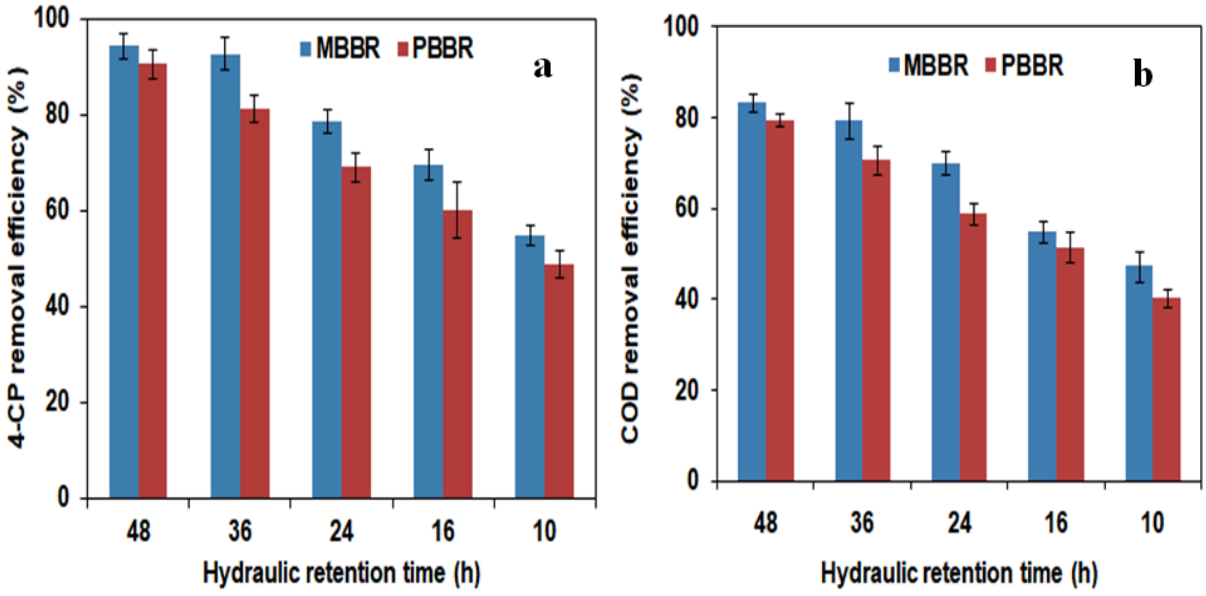


**Figure 4.23.** Effect of hydraulic retention time on (a) 4-CP, and (b) COD removal efficiency in MBBR and PBBR.

The REs of 4-CP and COD were found higher for the MBBR compared to the PBBR at a fixed HRT (Figure 4.24 (a, b)). The MBBR could be able to degrade 94.34 % of 4-CP while maximum RE in PBBR was obtained of 90.62 % at an HRT of 48 h. This could be attributed to the movement of the biocarriers in the MBBR, which enhances the diffusion of the substrate from bulk liquid to the bacterial cell. Moreover, the attached biomass concentrations were measured to be 508.07, 385.24 mg/L in MBBR and PBBR, respectively. Simultaneously, the MLSS was higher in the PBBR than the MBBR and was found to be 1105.42 mg/L at an initial concentration of 50 mg/L (Table 4.19). Although the microbial population present in the bioreactor was assumed to be in the growth phase, the dead and inactive microorganisms contribute to higher MLSS in PBBR and MBBR with no enhancement of 4-CP and COD REs.

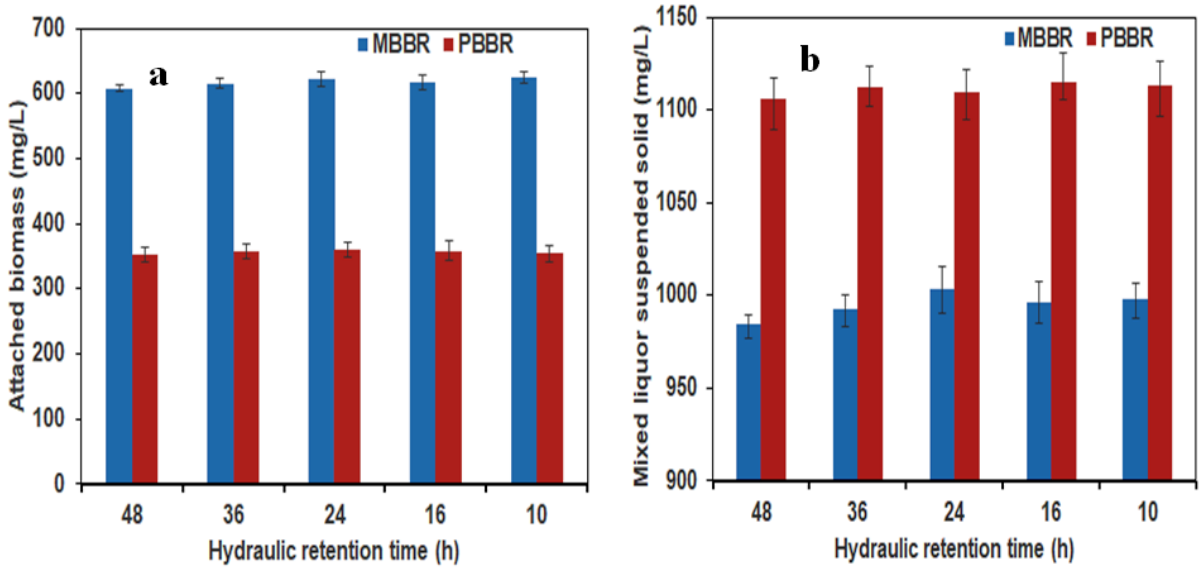


**Figure 4.24.** Effect of hydraulic retention time on (a) attached biomass, and (b) mixed liquor suspended solid in MBBR and PBBR.

### 4.14. Effect of 4-CP concentration and ILR on the performance of MBBR and PBBR

In the second stage, the bioreactors were operated with different ILRs (0.033 – 0.167 kg/m$^3$. d) by varying the initial 4-CP concentration from 50-250 mg/L at a fixed HRT of 36 h. The initial 4-CP concentration and ILR were set at 50 mg/L and 0.033 kg/m$^3$.d, respectively. The maximum REs of 4-CP were obtained to be 93.41 and 88.16 % for MBBR and PBBR, respectively. Similarly, the corresponding COD REs were determined to be 77.08 and 70.27 %. Then, the initial 4-CP concentration and ILR were subsequently increased to 100 mg/L and 0.067 kg/m$^3$.d, respectively. A slight decline of RE was observed in MBBR and PBBR. The maximum REs of 4-CP were obtained to be 90.75 and 81.65 % in MBBR and PBBR, respectively. When the ILR was increased to 0.1 kg/m$^3$.d by increasing the initial concentration of 4-CP to 150 mg/L, the maximum 4-CP REs were decreased to 81.61 and 68.08 % in the MBBR and PBBR, respectively. Similarly, the corresponding COD REs were obtained as 69.75 and 57.59 %. Further, the ILR was increased to 0.167 kg/m$^3$.d by increasing the concentration of 4-CP to 250 mg/L. The 4-CP REs gradually declined and

obtained 50.83 and 43.67 % in MBBR and PBBR, respectively. Similarly, the COD REs were sharply declined to 41.7 and 38.46 %, respectively. The REs of 4-CP and COD were gradually decreased with the increase of 4-CP concentration. The fixed biomass attached to the solid packing support can degrade a certain amount of the substrate within a specific time period. However, with the increase in substrate concentration, complete degradation will require more time (Basak et al., 2019; Farah et al., 2004).

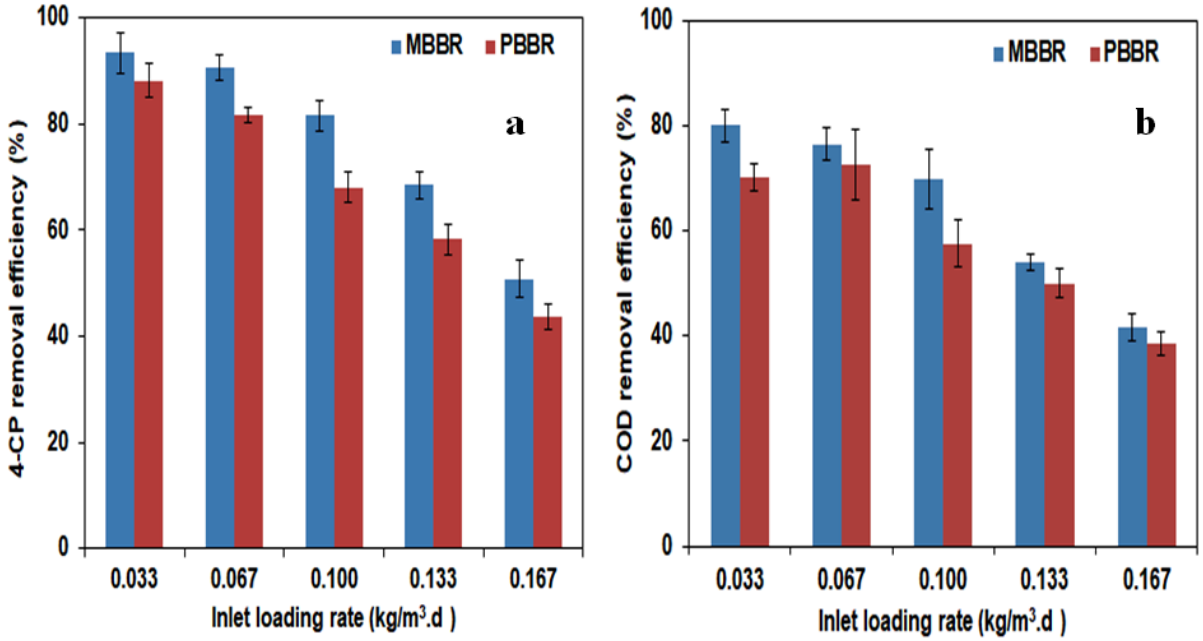


**Figure 4.25.** Effect of inlet loading rate and initial 4-CP concentration on (a) 4-CP, and (b) COD removal efficiency in MBBR and PBBR.

In this study, the MBBR offers high REs of 4-CP and COD compared to the PBBR (Figure 4.25). The MBBR shows more robustness towards biodegradation of 4-CP at high concentration due to the better substrate and oxygen diffusivity, which promotes higher biomass growth onto the PP-PUF biocarriers (Figure 4.26). The attached biomass was gradually increasing with the substrate concentration and obtained higher for MBBR. The attached biomass in MBBR and PBBR was found in the range of 482.18–532.81 mg/L and 379.21–431.31 mg/L, respectively. Rezaee et al., 2011 have performed a comparative

analysis between MBBR and PBBR with municipal wastewater and reported that the MBBR could perform better than the PBBR under identical conditions due to high biomass growth.

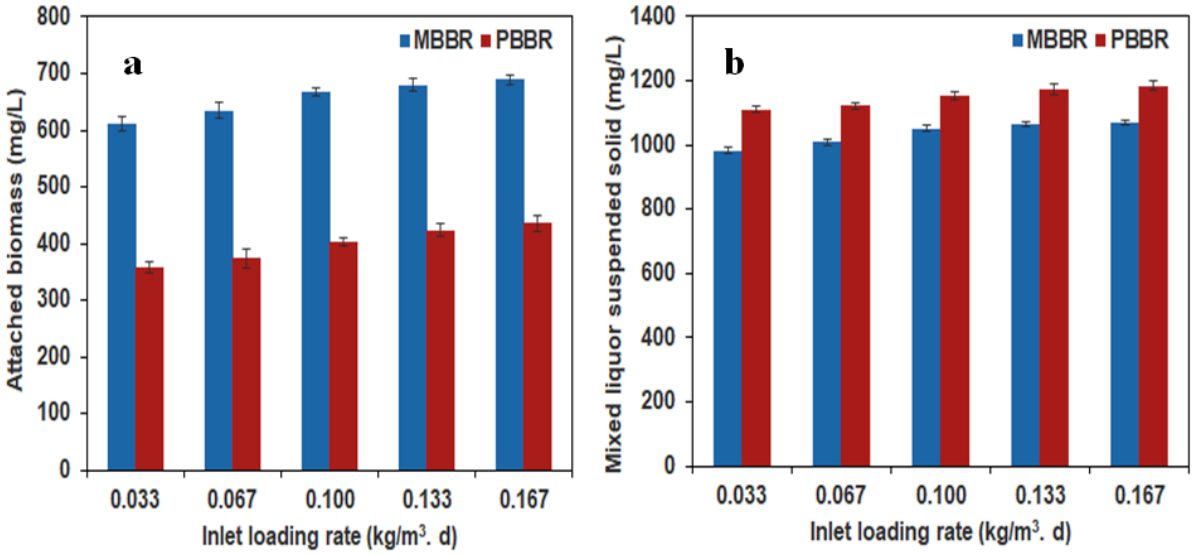


**Figure 4.26.** Effect of inlet loading rate on (a) attached biomass and (b) mixed liquor suspended solids in MBBR and PBBR.

**Table 4.18.** The summary of experimental results obtained from continuous operation of a moving bed bioreactor.

| Days of operation | HRT (h) | 4-CP concentration (mg/L) | ILR ($kg/m^3$. d) | 4-CP RE (%) | COD RE (%) | Attached biomass (mg/L) | MLSS (mg/L) |
|---|---|---|---|---|---|---|---|
| 0-20 | 48 | 50 | 0.025 | 94.34 ± 2.64 | 83.26 ± 5.81 | 608 ± 5.08 | 984 ± 6.91 |
| 21-36 | 36 | 50 | 0.033 | 92.75 ± 3.31 | 79.46 ± 3.92 | 615 ± 7.85 | 992 ± 9.28 |
| 37-53 | 24 | 50 | 0.05 | 78.61 ± 2.53 | 69.97 ± 6.65 | 621 ± 11.67 | 1003 ± 13.14 |
| 54-70 | 16 | 50 | 0.075 | 69.55 ± 3.19 | 54.89 ± 4.22 | 617 ± 10.59 | 996 ± 11.89 |
| 71-95 | 10 | 50 | 0.12 | 54.83 ± 2.20 | 47.18 ± 3.27 | 623 ± 8.35 | 998 ± 10.4 |
| 96-120 | 36 | 50 | 0.033 | 93.41 ± 3.76 | 80.08 ± 3.05 | 612 ± 12.67 | 983 ± 9.69 |
| 121-145 | 36 | 100 | 0.067 | 90.75 ± 2.45 | 76.51 ± 3.15 | 634 ± 13.21 | 1008 ± 7.97 |
| 146-162 | 36 | 150 | 0.1 | 81.61 ± 2.85 | 69.75 ± 5.64 | 667± 8.40 | 1052 ± 10.29 |
| 163-185 | 36 | 200 | 0.133 | 68.55 ± 2.51 | 53.90 ± 1.52 | 680 ± 10.98 | 1064 ± 8.95 |

| | | | | | | | |
|---|---|---|---|---|---|---|---|
| 186-210 | 36 | 250 | 0.167 | 50.83 ± 3.54 | 41.70 ± 2.53 | 689 ± 7.74 | 1069 ± 7.15 |

HRT: Hydraulic retention time; ILR: Inlet loading rate; RE: Removal efficiency; COD: Chemical oxygen demand; MLSS: Mixed liquor suspended solid.

**Table 4.19.** The summary of experimental results obtained from continuous operation of a packed bed bioreactor.

| Days of operation | HRT (h) | 4-CP concentration (mg/L) | ILR ($kg/m^3$. d) | 4-CP RE (%) | COD RE (%) | Attached biomass (mg/L) | MLSS (mg/L) |
|---|---|---|---|---|---|---|---|
| 0-20 | 48 | 50 | 0.025 | 90.62 ± 2.92 | 79.37 ± 9.39 | 351 ± 11.39 | 1105 ± 16.01 |
| 21-36 | 36 | 50 | 0.033 | 81.39 ± 2.86 | 70.53 ± 7.13 | 357 ± 10.75 | 1112 ± 10.93 |
| 37-53 | 24 | 50 | 0.05 | 69.16 ± 30 | 58.76 ± 5.39 | 360 ± 11.52 | 1109 ± 15.47 |
| 54-70 | 16 | 50 | 0.075 | 60.28 ± 5.85 | 51.48 ± 7.2 | 358 ± 15.75 | 1115 ± 9.44 |
| 71-95 | 10 | 50 | 0.12 | 51.91 ± 2.81 | 40.36 ± 4.01 | 354 ± 12.47 | 1113 ± 17.33 |
| 96-120 | 36 | 50 | 0.033 | 88.16 ± 3.24 | 70.27 ± 2.65 | 358 ± 9.80 | 1110 ± 9.23 |
| 121-145 | 36 | 100 | 0.067 | 81.65 ± 1.4 | 72.61 ± 6.58 | 373 ± 15.88 | 1121 ± 8.03 |
| 146-162 | 36 | 150 | 0.1 | 68.08 ± 2.94 | 57.59 ± 4.59 | 404 ± 7.19 | 1153 ± 11.17 |
| 163-185 | 36 | 200 | 0.133 | 58.23 ± 3.99 | 49.96 ± 2.75 | 423 ± 11.21 | 1171 ± 16.79 |
| 186-210 | 36 | 250 | 0.167 | 43.67 ± 2.06 | 38.46 ± 2.25 | 435 ± 13.60 | 1185 ± 13.5 |